Control of drug bioavailability using Hybrid Mesoporous Silica Nanoparticles

Giorgia Figari

Thesis to obtain the Master of Science Degree in

Chemistry

Supervisors: Prof. Dr. José Paulo Sequeira Farinha

Dr.ssa María Teresa Viciosa Plaza

Examination Committee

Chairperson: Prof. Dr.ssa Isabel M. Marrucho

Supervisor: Dr.ssa María Teresa Viciosa Plaza

Members of the Committee: Dr.ssa Madalena Dionisio

January 2021

Abstract

The poor water solubility of many drugs has emerged as one of the major challenges in the pharmaceutical world. Amorphous solid dispersions have been considered as the major advancement in overcoming limited aqueous solubility and oral absorption issues. The main drawback of this approach is that they can lack the necessary stability and revert to the crystalline form on storage. Significant upfront development is therefore, required to generate stable amorphous formulations. The objective of this work is to use mesoporous silica in amorphous oral drug delivery systems. In particular, the aim is to increase the bioavailability of a commercial drug, Fenofibrate, by promoting its amorphous state when confined in mesoporous silica nanoparticles (MSNs). MSNs nanovehicles with diameters under 100 nm were functionalized with different organic groups in the pores to tune the interaction of the drug with the matrix and thus avoid its crystallization which impairs bioavailability. This approach has the potential for application in different systems and offers two advantages: (i) provides a vehicle for controlled delivery and (ii) stabilizes the amorphous state, improving the solubility and bioavailability of the drug. The potential advantage of MSNs as inert, hydrophilic, pharmaceutical carrier matrices is discussed. A brief introduction to the Biopharmaceutical Classification System, nanoparticles and the solubility advantage of amorphous drugs is provided. In addition, the preparation, characterization and functionalization of MSNs for drug release are also presented. In the present study fenofibrate was loaded in a silica matrix with and without functionalization of their pores with two modifying agents that differs in hydrophilicity. Specifically, hydrophilic (3-Aminopropyl) triethoxysilane (APTES) and hydrophobic trimethoxy(phenyl)silane (TMPS). To access the physical state of fenofibrate inside the silica matrix, differential scanning calorimetry (DSC) was used. Dielectric relaxation spectroscopy (DRS) was used to probe the molecular mobility of the drug. The different techniques provided complementary information and reveal that drug incorporation inside a nanoporous matrix is a suitable strategy to stabilize fenofibrate in the amorphous state. Release studies were performed to analyze how the physical state of loaded fenofibrate into bare and functionalized mesoporous silica nanoparticles is reflected in the delivery.

Keywords: mesoporous silica nanoparticles, solubility, amorphous state, drug release, pore functionalization

Index

Index ..... **III**

1. Introduction **1**

1.1 Mesoporous silica as drug delivery systems 2

1.1.1 Characteristics 3

1.1.2 Synthesis 3

1.1.3 Surface Modification 5

1.2 Effect of MSNs Dimensions on The Stabilization of the drug amorphous state 8

1.3 Silica formulations of Fenofibrate 9

2. Experimental Section **10**

2.1 Materials 10

2.2 Equipment 11

2.3 Methods and Techniques 14

2.3.1 Synthesis of Mesoporous Silica Nanoparticles 14

2.3.2 Modification of the MSNs pores 14

2.3.3 Fenofibrate Loading in Mesoporous Silica Nanoparticles 16

3. Results and Discussion **18**

3.1 MSNs Synthesis and Characterization 18

3.2 Functional Groups 20

3.2.1 Identification by FTIR 20

3.2.2 Quantification by NMR 22

3.3 Fenofibrate loaded MSNs 25

3.3.1 Identification by FTIR 25

3.3.2 Quantification by NMR 28

3.3.3 Quantification by UV-Vis 30

3.4 Physical State of FNB in the MSNs 32

3.4.1 DSC Results 33
3.4.2 DRS Results 41
3.5 Release Study 50
4. Conclusions 53
5. Future studies 54
6. Bibliography 55

List of figures

Figure 1. Biopharmaceutics classification system and formulation approaches for different classes of drugs. (adapted from reference [3]) 1
Figure 2. Chemical structure of tetraethyl orthosilicate (TEOS). 4
Figure 3. Illustration of mesoporous material formation with surfactant (adapted from references [20]) 5
Figure 4. Versatility of MSN as a carrier in loading variety of drugs (adapted from references [14]) 6
Figure 5. Co-condensation and post synthetic functionalization. A trialkoxysilane molecule with a functional moiety (red) is shown as an example of a precursor. The templating agent is represented by the blue micelles adapted from references [25]). 6
Figure 6. Post synthetic functionalization scheme, exemplified by reaction of a trialkoxyorganosilane with the silanol groups of the surface of the mesoporous silica (adapted from [27]) 7
Figure 7. Co-condensation method functionalization. Using as precursor, a silica source and a terminal trialkoxyorganosilane for the organic modification (adapted from reference [27]) 7
Figure 8. Structure of fenofibrate (FNB) 10
Figure 9. Representative image of sample preparation for performing the release study: A – Dialysis device (with a cellulose membrane) containing 200 µL of PBS/EtOH(10%) with nanoparticles loaded with FNB , on top of a quartz cuvette and B – quartz cell containing 3.3 mL of PBS/EtOH(10%) 13
Figure 10. Chemical structure of 3-(aminopropyl)triethoxysilane (APTES) (left) and of trimethoxy(phenyl)silane (TMPS) (right). 15
Figure 11. Amine internal (A) and external (B) surface functionalization with APTES molecule (adapted from [44]) 15
Figure 12. Schematic functionalization with TMPS molecule adapted from [45]) 16
Figure 13 (a, b) TEM of the synthesized MSNs; (c) Histogram of the size distribution from the TEM data. The mean particle size is (49 ± 6.6) nm, based on 50 measurements. 19
Figure 14. FTIR spectra of pure APTES, bare MSNs and modified MSNs_APTES 21
Figure 15. FTIR spectra of pure functionalized agent (TMPS), bare mesoporous nanoparticles (MSNs) and modified mesoporous nanoparticles (MSNs_TMPS). 21
Figure 16. ^{1}H NMR spectra recorded of MSNs_APTES in NaOH/D_2O.The internal standard peak is at 5.15 ppm. Ethanol peaks are marked with (*). 22
Figure 17. ^{1}H NMR spectra recorded at 400 MHz of MSNs_TMPS in NaOH/D_2O. The internal standard peak is at 5.15 ppm. Ethanol peaks are marked with (*) (a). ^{1}H NMR spectra recorded for pure TMPS from the database (b) (guidechem.com) 24
Figure 18. FTIR spectra obtained for three MSN, unmodified, functionalized with APTES and functionalized with PTES, without and with fenofibrate. Grey rectangles identified the principal regions of FNB bands. 26
Figure 19. FTIR spectra of bulk FNB (orange) FNB@MSNs(red), FNB@MSNs_APTES (blue) and FNB@MSNs_TMPS (green) in the carbonyl stretching region. 28

Figure 20. ^{1}H NMR spectra of FNB@MSNs in $NaOH/D_2O$. The internal standard peak is at 5.15 ppm. The arrow indicates the considerate peaks (a). ^{1}H NMR from literature (b) (guidechem.com) 29
Figure 21. ^{1}H NMR spectra of FNB@MSNs in $NaOH/D_2O$. The internal standard peak is at 5.15 ppm. The arrow indicates the evaluated peaks at higher ppm regions (around 7.6 ppm) mL. 30
Figure 22. Absorption spectra of the diluted supernatants recovered after centrifugation of FNB@MSNs_APTES in EtOH. Supernatant 1 removed after the 1st centrifugation (green), supernatant 2 removed after the 2nd centrifugation (orange) and supernatant 3 removed after the 3rd centrifugation (blue)..... 31
Figure 23. Calibration curve of FNB solutions in EtOH 31
Figure 24. Thermograms of fenofibrate obtained on heating at 10 ºC/min: dotted line, on heating from room temperature up to 95 ºC; red line, upon cooling down to -50ºC and then heating up to 90°C. Green square indicates the glass transition region that it is enlarged in the inset (heating) showing the auxiliary lines (dotted) used to determine the onset, midpoint and endset of this transition. 33
Figure 25.Heating thermograms at 10 ºC/min of FNB@MSNs. Inset represents the temperature/time experimental procedure followed. 34
Figure 26. Heating thermograms at 10 ºC/min of the sample FNB@MSNs obtained with gradual heating. Left inset shows the enlarged glass transition range in the heating 1; Right inset represents the temperature/time experimental procedure followed. The final temperature of each cycle is: T_f 1=50°C; T_f 2=70°C; T_f 3=100°C; T_f 4=100°C 35
Figure 27. Heating thermograms at 10 ºC/min of FNB@MSNs_APTES. Inset represents the temperature/time experimental procedure followed. 36
Figure 28. Heating thermograms at 10 ºC/min of the sample FNB@MSNs_APTES obtained with gradual heating. Left inset shows the enlarged glass transition range in the heating 1. The final temperatures of each cycle are T_f 1=40°C; T_f2=50°C; T_f3=70°C; T_f4=100 ° C and T_f5 =100 °C 37
Figure 29. Heating thermograms at 10 ºC/min of the sample FNB@MSNs_TMPS obtained with gradual heating. Inset shows the enlarged glass transition region on heating 1 The final temperatures of each cycle are T_f 1 = 40°C; T_f 2 = 50°C; T_f 3 = 70°C; T_f4 = 100°C; T_f 5 = 100°C. 38
Figure 30. Heat flow change of FNB. Inset define the first heating up 50°C for FNB@MSNsand first heating up 40°C for FNB@MSNs_APTES and FNB@MSNs_TMPS. 40
Figure 31. M" *vs.* T plot at 10^5 Hz of MSNs (series 1 and 2) and MSN_APTES (series 1 and 2) representing the different amount of water that remain adsorbed on the silicas after the first heating up to 150°C. 41
Figure 32. ε´ vs. T plot at 0.1 Hz of: (a) MSNs and (b) MSNs_APTES; blue and red data correspond to series 1 (hydrated) and series 2 (dried) respectively. 42
Figure 33. Isochronal representation of M´´ *vs.* T at 10^5 Hz for native FNB (black squares), MSN_FNB series 1 (hydrated) in light blue, and series 2 (dried) in red. 43
Figure 34. Isochronal representation of M´´ *vs.* T at 10^5 Hz for native FNB (black squares), FNB@MSNs_APTES serie 1 (hydrated) in light blue, and series 2 (dried) in red. 44
Figure 35. Isochronal representation of M´´ *vs.* T at 1MHz, 6 x10^5 and 10^5 Hz of FNB@MSNs_APTES. 45

Figure 36. Isochronal representation of M´´ collected in the isothermal mode from -120 to 120°C covering the frequency range from 0.1 Hz up to 1 MHz for the sample FNB@MSNs in the second series. 45
Figure 37. Dielectric loss of fenofibrate versus temperature at a frequency of f = 95.241 Hz confined to the MSNs_FNB; the solid lines (red and green) are the two gaussian summed to simulate the isochronal plot of FNB@MSNsabove -50°C. the overall global fit is included (blue line) 46
Figure 38. Temperature dependence of the relaxation times of each process observed in: red symbols for bulk amorphous FNB (in this sample, the temperature position was taken directly from the M´´ *vs*. T representation, i.e., without mathematical deconvolution of peaks); blue symbols for MSNs_FNB, and green samples for FNB@MSNs_APTES. Solid lines correspond to the respective Arrhenius and VFTH curve fits. Dot lines show the T_g of amorphous FNB and a fix frequency for better comparison. 47
Figure 39. Release profile of FNB@MSNs_APTES (black line) and FNB@MSNs_TMPS (pink line) obtained at λ = 289 nm. 50
Figure 40. Absorption spectra of FNB solutions in PBS/EtOH at λ = 289 nm, inset shows the respective concentrations in [mol/L] (top) and corresponding calibration curve (bottom). $Abs = 15.2 \pm 0.5x103\ C + 0.005 \pm 0.003$ with r^2 = 0.996 51

List of tables

Table 1. Drug loading conditions 17
Table 2. APTES and TMPS concentration on the MSNs, calculated by ^{1}H NMR 24
Table 3.number of moles of FNB in the supernatants for each sample. 32
Table 4. FNB loading in the nanoparticles. 32
Table 5. Glass transition temperature at the onset, midpoint and end point obtained on successive heatings of the sample FNB@MSNs during the gradual drying treatment and respective heat capacity. 36
Table 6. Glass transition temperature at the onset, midpoint and end obtained on successive heatings of the sample FNB@MSNs_APTES during the gradual drying treatment and respective heat capacity. 38
Table 7. Glass transition temperature at the onset, midpoint and end obtained on successive heatings of the sample FNB@MSNs_TMPS during the gradual drying treatment and respective heat capacity. 39
Table 8. T_g onset values of FNB in bare MSNs, MSNs_APTES and MSNs_TMPS under gradual heating until 70°C, [b] up to 100°C 39
Table 9. Glass transition temperatures, activation energy and $\tau\infty$ values for native drug, FNB@MSNs and FNB@MSNs_APTES determined from dielectric data. 48
Table 10. FNB released after 8 hours 52

List of Abbreviations

Abs- Absorbance

APTES- (3-Aminopropyl) triethoxysilane

CTAB- Hexadecyltrimethylammonium Bromide

^{1}H NMR- Proton Nuclear Magnetic Resonance

DSC- Differential scanning calorimetry

DMSO- Dimethyl sulfoxide D6

ε´- Permittivity (real part)

ε- Molar absorption coefficient

FNB- Fenofibrate

FTIR- Fourier Transform Infrared Spectroscopy

M´´- Dielectric modulus

MSNs- Mesoporous Silica Nanoparticles

MSNs_APTES- Mesoporous Silica Nanoparticles Surface Modified with APTES

FNB@MSNs- Mesoporous Silica Nanoparticles containing FNB

FNB@MSNs_APTES- Mesoporous Silica Nanoparticles Surface Modified with APTES and containing **FNB**

MSNs_TMPS- Mesoporous Silica Nanoparticles Surface Modified with TMPS

FNB@MSNs_TMPS- Mesoporous Silica Nanoparticles Surface Modified with TMPS and containing FNB

η- Viscosity

R- Gas constant

TEOS- Tetraethyl ortohosilicate

TEM- Transmission Electron Spectroscopy

T_g- Glass transition temperature

TMPS- Tetramethoxy (phenyl) silane

UV-VIS- UV-Vis Spectroscopy

Unit List

℃- Degree Celsius

g; mg- Grams; milligrams (10^{-3} g)

h; min; s- hours; minutes; seconds

L; mL; µL- Litre; millilitre (10^{-3} L); microlitre (10^{-6} L)

m, cm, µm, nm- meter; centimeter (10^{-2} m); micrometer (10^{-6} m); nanometer (10^{-9} m)

MHz- Megahertz

mol; mmol- Mol; millimol (10^{-3} mol)

rpm- Rotations per minut

1.INTRODUCTION

The most common route of drug administration is the oral one. Among other advantages, it has high patient compliance, cost effectiveness and flexibility of dosage from design. [1] As a result, many of the generic drug companies are more inclined to produce bioequivalent oral drug products. However, the major challenge with the design of oral dosage forms lies with the poor bioavailability of many pharmaceutics. Oral bioavailability depends on several factors including aqueous solubility, drug permeability, dissolution rate, first-pass metabolism, presystemic metabolism, and susceptibility to efflux mechanisms. The most frequent causes of low oral bioavailability are attributed to poor solubility and low permeability. [2] Solubility is one of the important parameters to achieve the desired concentration of drug in systemic circulation for pharmacological response, and consequently it represents a major challenge for formulation. Currently, more than 40% new chemical entities (NCEs) developed by the pharmaceutical industry are practically insoluble in water which limits their use. [2] Thus, the solubility problems complicate the delivery of these new drugs and also affect the delivery of many existing drugs. Amidon et al.[3] classified active pharmaceutical ingredients (APIs) into four groups based on their solubility and permeability known as the Biopharmaceutical Classification System (BCS) (Figure 1). According to the US Food and Drug Administration (FDA), a drug is considered to be highly soluble when its highest clinical dose is soluble in ≤250 mL of aqueous media over a pH range of 1-7.5 at 37.5°C. It is considered to be highly permeable if the absorption of an orally administered dose in humans is >90% when determined using mass balance or in comparison to an intravenous reference dose. [3]

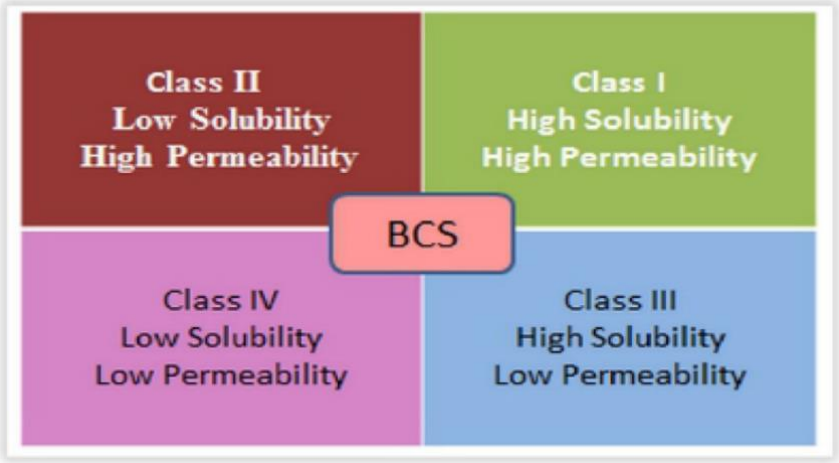

Figure 1. Biopharmaceutics classification system and formulation approaches for different classes of drugs. (adapted from reference [3])

The poor solubility and low dissolution rate of poorly water-soluble drugs in the aqueous gastrointestinal fluid often cause insufficient bioavailability. According to the BCS, the bioavailability may be enhanced

by increasing the solubility and dissolution rate of the drug in the gastrointestinal fluids. In addition, the concept of BCS provides a better understanding of the relationship between drug release and the absorption process. [4] For instance, BCS class II drugs have low solubility and high permeability, i.e. the limiting step is the drug release and the solubility in the gastric fluid, not the absorption. In this case, increasing the solubility is expected to increase the bioavailability. Therefore, there is great interest to develop reliable, efficient, cost effective, and scalable methods to increase the aqueous solubility of BCS class II drugs. Various techniques are used for the enhancement of the solubility of poorly soluble drugs which include physical (such as particle size reduction or crystal engineering) [2], and chemical methods (such as salt formation [5], complexation, or ionic liquid synthesis). The choice of a particular method depends mainly on the physicochemical characteristics of drugs, carrier properties, and their expected uses. Regarding the internal structure, a solid can exist in a crystalline or amorphous form. If a substance can exist in more than one crystalline structure, they are designed polymorphs, and the phenomenon is known as polymorphism. [6] Dissolution and performance of the drug depend on its physicochemical properties in such a way that different polymorphs have different apparent aqueous solubility and dissolution rate. Such differences will change the bioavailability of the drug. Thus, it is often difficult to formulate a bioequivalent drug product using a different polymorph.

One of the polymorphic forms are usually physically more stable than the others. Such a stable polymorph represents the lowest energy state, which has the highest melting point and least aqueous solubility. The remaining polymorphs are called metastable forms being less thermodynamic stable. [6] The most stable polymorphic of a drug is often used because of its stability. Nevertheless, other polymorphs can be used in alternative if they present enhanced bioavailability. [7] On the other hand, solid-state manipulation by amorphization of poorly water-soluble compounds also represents a possible strategy to enhance the dissolution rate. It has been shown that the amorphous state can improve the drug release rate, both in vitro and in vivo, relatively to its crystalline counterpart. [8] This is due to a higher free energy of the amorphous state compared to the crystalline state, which may act as a driving force leading to higher apparent water solubility, dissolution rate, and oral absorption. Commonly used techniques to produce the amorphous form of drugs include the formation of solid drug dispersions with water-soluble carriers, co-grinding with additives, melt-extrusion, melt quenching, or spray drying. [9] However, commercial applications of some of these techniques have been constrained, primarily due to the challenges in stabilizing the amorphous form of drugs in these systems. [10] In fact, the amorphous is out of thermodynamic equilibrium, and therefore may convert to the more stable thermodynamic form, i.e. it can recrystallize.

1.1 MESOPOROUS SILICA AS DRUG DELIVERY SYSTEMS

First synthesized by Mobil corporation scientists in 1992 [11], ordered mesoporous silica recently became a new generation of inorganic platform for biomedical application. Different from the conventional materials with heterogeneous porosity, mesoporous silica has a homogeneous structure

with nanoscale channels as per IUPAC, mesoporous materials are defined as having a pore size in the range of 2–50 nm and an ordered arrangement of pores. With huge surface area and ordered porous interior, mesoporous silica can be used as versatile host for a variety of pharmaceutical agents, and subsequently provide pathways for diffusion. Mobil Crystalline Materials (MCM-41) were reported as the first mesoporous silica drug carrier in 2001 with an ordered arrangement of uniform hexagonal mesopores. [11] Apart from this, various other materials of mesoporous nature have also been synthesized by varying the starting precursors and reaction conditions.

1.1.1 CHARACTERISTICS

In recent years, there has been a growing interest in the use of ordered mesoporous silica as a drug carrier for poorly soluble drugs. [12] Mesoporous silica materials offer several attractive features, which render them excellent candidates for controlled drug delivery systems. First, an environment potentially suitable for adsorption of small and large molecules can be created by varying their pore sizes between 2 and 30 nm. The pore size can determine the size of molecules that can be loaded into the carrier. The pore/cargo size ratio should be higher than unity so that the pore is accessible to the drug molecule. [13] However, pore size is not the only factor that must be considered when designing this type of nanocarriers.

Second, the particles have a large surface area for drug adsorption and a high pore volume for drug confinement. Third, the silanol groups can be functionalized to modify drug binding and finally, drugs can be homogenously distributed and stabilized in the amorphous state or in different crystalline arrangements inside the ordered matrix. [14] Furthermore, the most remarkable advantage of MSNs materials as drug delivery systems is their “zero premature controlled release” property. Namely, drugs are carried with precise control of location and time without leaching prior to reaching the targeted cells or tissues and this will reduce drug dosage and side effects. [15]

In other words, MSNs can level off the drug concentration at the targeted area as the release of the drug molecules form the ordered pores is controlled by a tunable diffusion at the target site over a period of time and this will reduce drug dosage and side effects. [16]

The high surface area and total pore volume, together with the chemical mechanical resistance of MSNs, protect materials from the surrounding environment. MSNs are composed by an amorphous matrix of silica (SiO_2) with nanometric size pores ordered in different arrangements, depending on the synthesis process. The different morphology-controlled synthesis of silica nanoparticles defines the potential role of these materials in multiple applications. [17]

1.1.2 SYNTHESIS

Mesoporous silica nanoparticles (MSNs) are gaining importance as nanocarriers of molecules, polymers and biomolecules due to their ideal structural properties and surface chemistry. However, it is a

challenge to find a simple, sustainable, and scalable synthetic process to tune their diameter in the range of a few tens of nanometers, with narrow size dispersity. [18] Generally, a modified Stober 'sol-gel process' is used to produce MSNs with controlled mesopore structure and surface properties. The sol-gel process involves the hydrolysis and condensation of the alkoxide monomers into a colloidal solution (sol), which acts as a precursor to form an ordered network (gel) of discrete particles in basic medium. [19] The most commonly used silica alkoxide is tetraethyl orthosilicate (TEOS) (Figure 2).

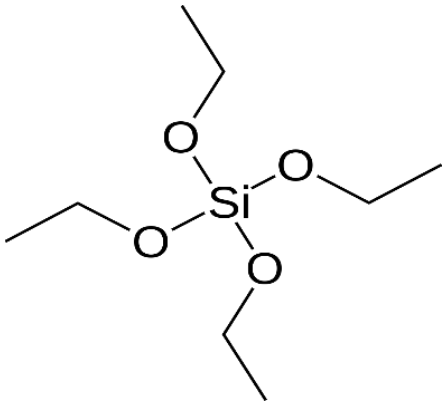

Figure 2. Chemical structure of tetraethyl orthosilicate (TEOS).

The general reactions of TEOS that leads to the formation of silica particles in the sol-gel process are:

(1) $Si(OCH_2CH_3)_4 + 4\ H_2O \leftrightarrow Si(OH)_4 + 4\ CH_3CH_2OH$
(2) $Si(OCH_2CH3)_4 + Si(OH)_4 + 3H_20 \leftrightarrow (OH_3)Si\text{-}O\text{-}Si(OH_3) + 4CH_3CH_2OH$
(3) $Si(OH)_4 + Si(OH_4) \leftrightarrow (OH_3)Si\text{-}O\text{-}Si(OH_3) + H_2O$

The hydrolysis of TEOS molecules forms silanol groups (1).
The condensation/polymerization between the silanol groups (3) or between silanol groups and ethoxy groups (2) creates siloxane bridges (Si–O–Si) that form entire silica structure. [20] The synthesis of mesoporous silica nanoparticles (MSNs) requires a surfactant such as cetyltrimethylammonium bromide (CTAB) in order to act as a template, a silica precursor such as tetraethyl orthosilicate (TEOS) or sodium metasilicate, and a base catalyst. The surfactant has an amphiphilic molecular structure (it consists of a hydrophobic (apolar tail) and a hydrophilic group (polar head)). In the synthesis process, when the concentration is higher than the critical micelle concentration (CMC), the surfactant spontaneously associates in solution forming a variety of structures, for example cylindrical (Figure 3). The shape of a surfactant molecule can be rationalized by its surfactant packing parameter. The packing parameter takes into account the volume of the hydrophobic chain, the equilibrium area per molecule at the aggregate interface, and the length of the hydrophobic chain.
The different structures not only depend on the packing parameter but also on the concentration, pH, temperature, etc. The precursor of silica condenses on the polar heads constituting the micelles and after removal of the surfactant, by calcination or acid extraction, mesoporous particles are obtained.

These nanoparticles are biocompatible and the three-dimensional network with silanol groups (= Si-OH) inside the pores or on the surface, and siloxane (= Si-O-Si =) inside the network, attribute the hydrophilic characteristic to the particles. [15] Moreover, by controlling the parameters during the synthesis, the morphology, pore size and volume and particle size can be transformed accordingly. [21]

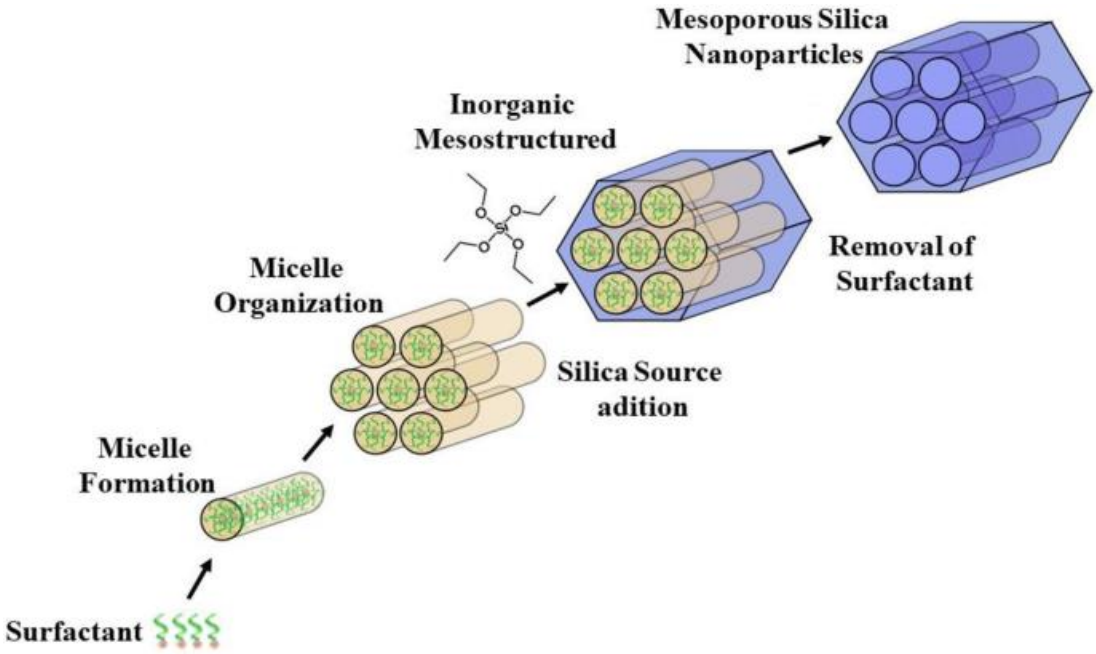

Figure 3. Illustration of mesoporous material formation with surfactant (adapted from references [20])

It is worth mentioning that the effects of the key reaction conditions (e.g., amount of TEOS, pH value, and reaction time) on the resulting MSNs were investigated, and it was concluded that the pH value is the dominant parameter influencing particle size. This is due to the stability of the micelles in the reactional medium. At high pH values there will be more OH- groups (after TEOS hydrolysis) to interact with the positive charges at the micelles surface, decreasing their stability. This charge screening induces the micelle aggregation, increasing the supramolecular aggregation number, and producing larger nanoparticles. [18,22]

1.1.3 Surface Modification

Another advantage of MSNs is the ease with which they can be functionalized to meet the requirements for a wide variety of applications. Figure 4 shows a pictorial representation depicting the versatility of MSNs carrier.

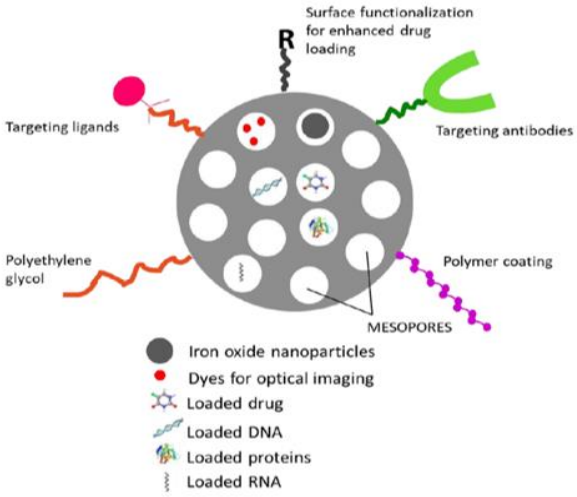

Figure 4. Versatility of MSNs as a carrier in loading variety of drugs (adapted from references [14]).

Functional groups can be used: (a) to control the surface charge of MSNs, (b) to chemically link with functional molecules inside or outside the pores and (c) to control the size of pore entrance for entrapping molecules in the nanopores. [23] Functionalization can be used to increase the loading of the molecules and to improve the interparticle and molecular interactions by consequently improve stability and biocompatibility. [24]

Functionalization can be performed by different approaches, either by co-condensation or by post synthetic methods (Figure 5). One of them consist in introducing organosilanes simultaneously with silica precursors during the synthesis of MSNs materials ("co-condensation"). The other pathway is to prepare unfunctionalized MSNs materials and subsequently to modify their surfaces with organosilanes ("grafting process").

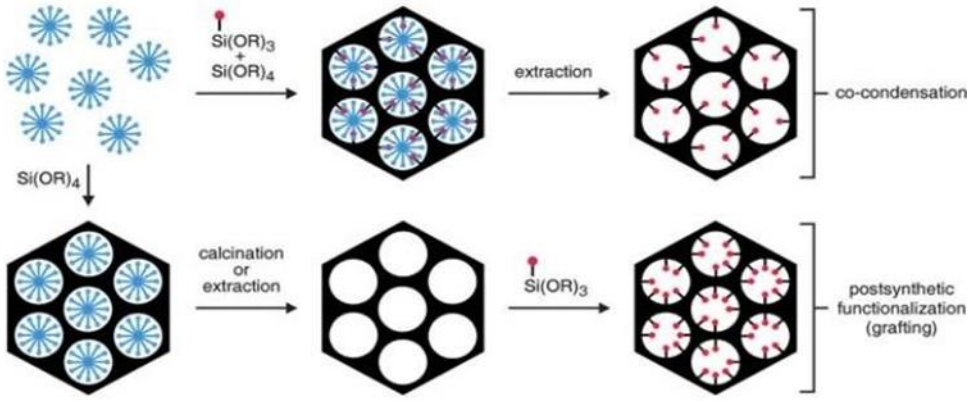

Figure 5. Co-condensation and post synthetic functionalization. A trialkoxysilane molecule with a functional moiety (red) is shown as an example of a precursor. The templating agent is represented by the blue micelles adapted from references [25]).

The grafting method has the disadvantage that it can be difficult to achieve a homogeneous distribution of the organic group due to the fact that major functionalization reactions take place between organic precursors and free silanol groups at the exterior surface and at the opening of the pores of MSNs. [26] However, taking advantage of this feature; it is possible to selectively functionalize the external and internal surfaces with different functional groups by maintaining and/or removing the surfactant. [25] Moreover, compared to the co-condensed material, organosilanes grafted MSNs materials have better retained pore structures and are more thermally stable. Figure 6 presents a post synthetic functionalization scheme.

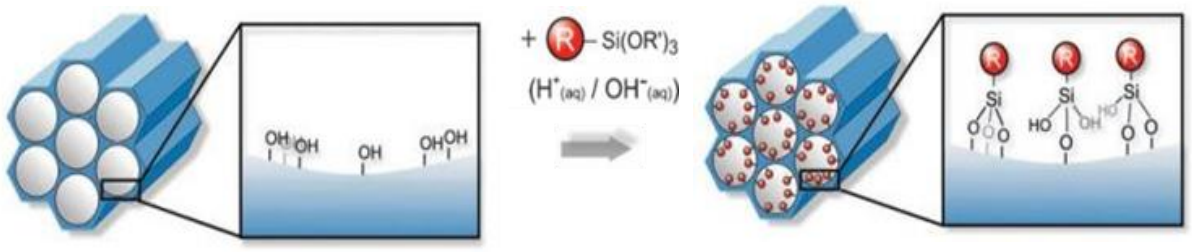

Figure 6. Post synthetic functionalization scheme, exemplified by reaction of a trialkoxyorganosilane with the silanol groups of the surface of the mesoporous silica (adapted from [27]).

The co-condensation method. (Figure 7) consists in adding an organosilanes precursor with a terminal functional group along with silica precursor and templating agent, into the reaction. Thus, by applying this method it is possible to obtain a more homogeneous distribution of the functional groups as they are components of the silica network. [28]

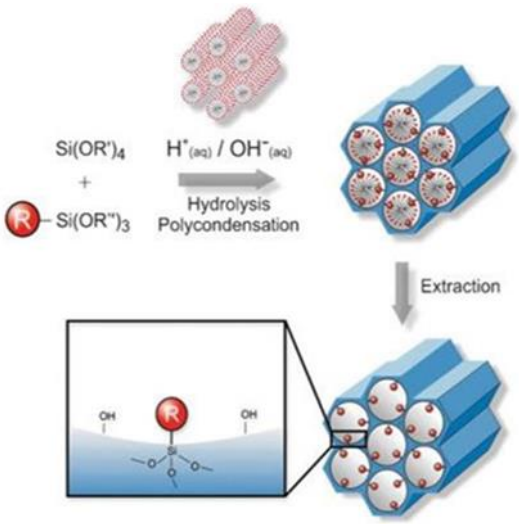

Figure 7. Co-condensation method functionalization. Using as precursor, a silica source and a terminal trialkoxyorganosilane for the organic modification (adapted from reference [27]).

Moreover, using the co-condensation method it is possible to control mesoporous silica nanoparticle morphology by the introduction of different organosilanes that will interact in a different manner with the surfactant molecules. [29]

Lin and coworkers [25] demonstrated that organosilanes with hydrophobic groups tend to intercalate their organic groups into the surfactant micelles and interact with the hydrophobic tails of surfactants, thus stabilizing the formation of long cylindrical micelles and giving rise to rod-shaped MSNs materials. However, the organic group can also destabilize the micelles during the formation of MSNs if the functional group is more hydrophilic, since surfactant interaction with polar group are not favored because they inhibit micelle growth and yield spherical particles with randomly oriented pore structures.[25]

1.2 EFFECT OF MSNs DIMENSIONS ON THE STABILIZATION OF THE DRUG AMORPHOUS STATE

Converting crystalline drugs into an amorphous form is one the most promising tool to overcome the problem of poor solubility, and it represents an alternative to more common approaches such as micronization of drugs or salt formation which has many practical limitations. [5]

The process of amorphization of the drug substance involves disruption of the ordered structure of a crystal which can be achieved by using a process like melt cast, hot melt technology and spray drying. Hence, amorphous drug exists in a higher free energy state and it has higher mobility as compared to its crystalline counterpart. Thus, the thermodynamic properties of amorphous state may result favorable to obtain a higher apparent solubility and dissolution rate. However due to high internal energy and enhanced molecular mobility of amorphous substances, they tend to crystallize during storage and dissolution. [30]

To benefit from the amorphous state, efforts have been made to reduce the driving force of recrystallization. For example, Beiner et al. [31] and Graubner et al. [32] shown that it is possible to stabilize substances in the amorphous state by incorporating in mesoporous matrix due to the confinement inside the pores that may prevent the rearrangement of the amorphous molecules into long-range order.

In brief, amorphization of a compound loaded on the mesoporous materials occurs through the limitation of space i.e. if the pore size of the mesoporous material is smaller than the critical nucleation size, it will eventually lead to stabilization of the amorphous drugs by decreasing mobility of the drug molecule that will have less tendency to organize in definite manner and thus form a crystal lattice structure. [33]

1.3 SILICA FORMULATIONS OF FENOFIBRATE

Fenofibrate (propan-2-yl 2-(4-[(4-chlorophenyl) carbonyl] phenoxy)-2-methylpropanoate) has been prescribed to treat hypercholesterolemia since 1970. It is a prodrug in which fenofibric acid is the active form. The pharmacological effect of fenofibrate (FNB) is to reduce low-density lipoprotein (LDL) and increase high-density lipoprotein (HDL) by binding to peroxisome proliferator-activated receptor alpha (PPARα). FNB is categorized as a BCS class II drug because of its poor aqueous solubility (0.8 μg/mL), and its high permeability (>90%) through lipid membranes. [34]

Two FNB polymorphs have been documented in the Cambridge Structural Database (CSD). The stable form I (with a melting point at 80°C) is the standard polymorph used as API in commercial tablets and capsules. Form I can be obtained by a slow solvent evaporation method. The metastable form called form II was reported by Di Martino et al. [35] It was produced by the recrystallization of amorphous FNB obtained from the melt. The melting point of the product was 74°C. It converts to the stable form I during heating via melt recrystallization.

Thus, with the increased use of the amorphous state of the drug in dispersions-based formulations, it is extremely important to fully understand the stability and crystallization behavior of amorphous FNB.

Zhou and co-workers have conducted a systematic study of a range of low-molecular weight drugs including FNB probing the relationship between physical stability and a range of thermodynamic properties. [36] They identified two important properties: molecular mobility, which is a measure of the rate of cooperatively rearrangement in subsystems in the amorphous state, and configurational entropy, which is the entropy difference between the disordered state and the crystalline one. The study revealed that the molecules that have high configurational entropies and low molecular mobilities were the ones that might not spontaneously recrystallize. In amorphous FNB the configurational entropy has a relatively high value, but it also exhibited a relatively high molecular mobility value. [37,38]

To overcome the solubility issue, particle size reduction (micronized and nanocrystals) and lipid dispersions have been used in the commercialized formulations containing FNB. [39] Sanganwar et al.[40] shown as FNB adsorbed onto the surface of silica reveals an increase in the dissolution rate. Adsorption was done first dissolving the drug in supercritical carbon dioxide and then depressurizing the solution onto silica. Since solvents are not used in the loading process, the silica formulation is free of any residual solvent, and carbon dioxide is freely removed upon depressurization. The improved dissolution in in vitro essays was attributed to increase in the surface area and decrease in the crystallinity of drug after adsorption onto silica.

It has been reported recently that some concentration-enhancing polymers can significantly improve drug bioavailability because they may inhibit nucleation or crystal growth by adsorption on the crystal interface thereby blocking crystal growth.

Jia et al. [41] prepared a formulation for oral administration of FNB from microparticles of silica with nanoporous around 18 nm (Sylysia®350) combined with a pH-sensitive polymethylmethacrylate (Eudragit® L100-55). The drug was incorporated by rotatory evaporation method. The improved

bioavailability observed in in vitro and in vivo tests was associated to the huge surface area of the mesoporous silica in which the drug is stabilized in a molecular or amorphous state.

Another approach, presented by Quan and co-workers [42], is based in the use of mesoporous silica matrix (SBA-15 with pore diameter close to 9 nm) to develop a solid self-emulsifying matrix with FNB incorporated. Their starting hypotheses consisted in simultaneously entrapping excipients and drug in the inert SBA-15 matrix. X-ray diffraction analysis does not show signal of crystalline FNB which leads to assume an amorphous or molecular state of FNB in the samples. From the comparison with commercial capsules, this formulation revealed and improved release rate and an enhanced bioavailability. Having in mind the success of using silicas for improving the poor water solubility of fenofibrate, the main objective of this work consists in the synthesis of mesoporous silica particles with pore diameter in the nanometer scale. In a second step, the pore surface was modified with two different groups in order to tune the interaction of the drug within the matrix, and thus stabilize Fenofibrate in its amorphous state, leading to an increase in solubility.

2. EXPERIMENTAL SECTION

2.1 MATERIALS

Fenofibrate (FNB), IUPAC name propan-2-yl 2-[4-(4-chlorobenzoyl)-phenoxyl]-2-methylpropanoate, (CAS number 49562-28-9), was purchased from Sigma-Aldrich (purity ≥ 99 %) and it was used without further purification. The empirical formula is $C_{20}H_{21}O_4Cl$ and the molecular weight is 360.83 g/mol. The chemical structure is presented in Figure 8.

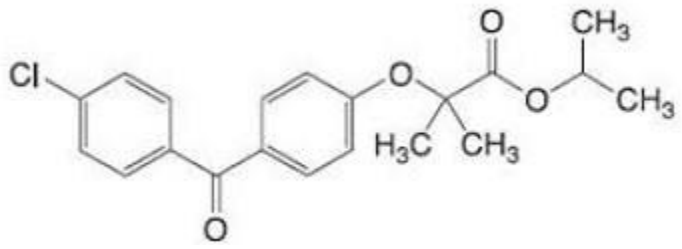

Figure 8. Structure of fenofibrate (FNB)

Absolute ethanol (EtOH,>99.9% Scharlau), tetraethoxysilane (TEOS, ≥99%, Aldrich), cetyltrimethylammonium bromide (CTAB, ≥99%, Sigma) and sodium hydroxide solution (NaOH 1,4 M) were used without any purification in the synthesis of mesoporous silica nanoparticles. For the removal of the surfactant a solution of 0.5 M hydrochloric acid (HCl, 37% Panreac) in absolute ethanol was used.

The deionized water was produced from a Millipore system Milli-Q ≥18 MΩcm (with a Millipak membrane filter 0.22 µm). Regarding nanoparticles functionalization, they were surface modified with trimethoxy(phenyl)silane (97% TMPS, Sigma Aldrich) and (3-Aminopropyl) triethoxysilane (98% APTES, Sigma-Aldrich) without any treatment in dried toluene which was distilled over calcium hydride before use. For NMR analysis samples was used 1,3,5-trioxane (≥99.0%, Fluka), deuterium oxide (D_2O, 99.9% atom, CIL) and dimethyl sulfoxide D6 (DMSO, 99,9%, CIL). disodium hydrogen phosphate (NaH_2PO_4, 99%, Riedel-de-Haën) and sodium dihydrogen phosphate monohydrate ($NaH_2PO_4.H_2O$, 98%, Panreac) were used to prepare the phosphate buffer solution (PBS, pH 8) for the release studies.

2.2 EQUIPMENT

Centrifuge

An Avanti J-301 (Beckman Coulter) was used for cleaning MSNs after template removal. For the centrifugations, 50 mL centrifuge propylene tubes were used. A Sigma 2k15 (B. Braun) centrifuge, rotor 12141, was used for washing functionalized MSNs at 1100 min^{-1}. Disposable 10 mL polypropylene tubes were used for the centrifugations. A Hitachi Himac CT 15RE centrifuge was utilized with 2 mL eppendorf for washing bare and functionalized nanoparticles after drug loading at 150 rpm.

Transmission Electron Microscopy (TEM)

TEM images were obtained on a Hitachi transmission electron microscope (Hitachi High – technologies, Tokyo, Japan), model H-8100, with a LaB6 filament (Hitachi) with an accelerator voltage of 200 kV. A camera KeenView (Soft Imaging System, Münster, Germany) is incorporated in this equipment, which through iTEM software, allows acquiring TEM images. MSNs dispersed in ethanol were prepared and dried on a copper grid coated with carbon. The size/dimension, polydispersity, and morphology of the particles were estimated by evaluating at least 50 nanoparticles by Image J software.

Fourier Transform Infrared Spectroscopy (FTIR)

Fourier Transform Infrared Spectroscopy (FTIR) spectra of pure organosilanes, crystalline FNB and FNB loaded in bare and functionalized MSNs were collected on a Bruker (model: Alpha) over the range 400-4000 cm^{-1} at room temperature. The samples were properly mixed with potassium bromide (KBr) in a mortare and pestle to form homogeneous mixture and punched using a KBr press.

Differential Scanning Calorimetry (DSC)

The thermal features were examined using differential scanning calorimeter DSC Q2000 from TA Instruments Inc. (Tzero DSC technology) operating in the Heat Flow T4P option. Enthalpy (cell constant) and temperature calibration were based on the melting peak of indium standard (T_m=156.60 °C). Approximately 5 mg of each sample were introduced in an aluminum hermetic pans with a Tzero hermetic lid with a pinhole to facilitate the exit of water. Thermograms of all the samples were obtained over a range of -90°C to 120°C at a heating rate of 10°C/min under a nitrogen flow of 50 mL/min and they were analyzed during heating. Then, the analysis of data was carried out using the software Universal Analysis 2000 from Thermal Analysis. Melting point (T_m) was determined as the minimum of the endothermic peak, whereas glass transition temperature (T_g) was determined at the onset of the glass transition.

Dielectric Relaxation Spectroscopy (DRS)

Dielectric measurements were carried out using the ALPHA-N impedance analyzer from Novocontrol Technologies GmbH, covering a frequency range from 0.1 Hz to 1 MHz. The sample powder was placed between two gold-plated electrodes of a parallel plate capacitor, BDS 1200 with two 50 um-thick silica spacers, the sample cell was mounted on a BDS 1100 cryostat and exposed to a heated gas stream being evaporated from a liquid nitrogen dewar. The temperature was controlled by Quatro Cryosystem and performed within 0.5 K. The dielectric relaxation spectra were collected on heating from -150°C up to 150°C regarding the unloaded nanoparticles and up to 120 °C for samples with fenofibrate in order to avoid degradation of the guest. Temperature was increased in different steps: from – 150°C to 50°C in steps of 5°C and in the remaining temperature range, every 2°C.

^{1}H NMR

Proton Nuclear Magnetic Resonance (^{1}H NMR) spectra were recorded on an AMX-400 instrument (Bruker, MA, USA) at 400 Mhz. For this purpose, two solutions of NaOH and 1,3,5-trioxane (internal standard, IS) in D_2O were prepared. In order to assess and quantify the quantity of FNB, APTES and TMPS, ^{1}H NMR was performed. In an NMR tube, 5 mg of particles, 400 µL of a solution of NaOH and 100 µL of a solution of 1,3,5-trioxane were mixed and sonicated.

UV-Vis Spectroscopy

UV-VIS spectra measurements were performed at room temperature with a UV-660 UV-VIS Spectrophotometer (JASCO International, Tokyo, Japan), with a double monochromator and a photomultiplier detector for higher resolution, was employed for UV-Vis spectroscopy assays at room temperature using MSNs samples dispersion in a quartz cuvette with 1 cm x 1 cm dimension and a polypropylene dialysis device with a cellulose membrane (Slide-A-Lyzer Mini Dialysis Devices, 10K MWCO, 0.5 mL) (Figure 9). For the release studies 1.73 mg of FNB@MSNs_APTES and 1.63 mg of FNB@MSNs_TMPS were placed in the dialysis membrane with a solution of PBS/EtOH(10%)

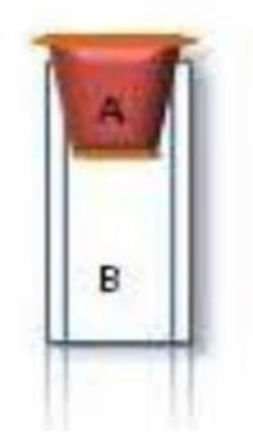

Figure 9. Representative image of sample preparation for performing the release study: A – Dialysis device (with a cellulose membrane) containing 200 µL of PBS/EtOH(10%) with nanoparticles loaded with FNB , on top of a quartz cuvette and B – quartz cell containing 3.3 mL of PBS/EtOH(10%)

pH

The pH of the phosphate buffer solution for the release studies was measured with a pHenomenal®,1000L bench pH/mV/°C meter pH.

2.3 METHODS AND TECHNIQUES

2.3.1 SYNTHESIS OF MESOPOROUS SILICA NANOPARTICLES

Silica mesoporous nanoparticles (MSNs) were synthesized by the sol-gel method. In a polypropylene flask with flat bottom 1.75 mL NaOH 1.4 M and 240 mL H_2O milli-Q were mixed. The mixture was transferred in an oil bath and heated to 32°C. The reaction was done in homogeneous stirring in order to have a stable mixture and avoid a larger distribution of diameters. Afterwards, 500 mg of CTAB were added to the solution and maintained under stirring for 30 min. Then, 2.5 ml of TEOS were added, drop by drop, and the solution was kept under continuous stirring for 3h at 35°C. The solution turned opaque almost immediately, indicating that the reaction has started. After cooling, the dispersion was put in polypropylene tubes with a capacity of 50 mL and centrifuged at 30000 G (Sigma 2k15 centrifuge, rotor 12141) for 15 minutes. Subsequently, the MSNs were washed 3 times with a solution of ethanol and water (50% V/V) to remove the excess of CTAB in the surface and in solution. The nanoparticles were dried in the oven at 50°C overnight. Then, 0.5 M HCl\ethanol (25 ml per 500 mg of MSNs) was added to solubilize the CTAB and the solution was sonicated for 15 minutes and left overnight stirring at 50°C. After the 24 hours the particles were washed 3 times. The first wash was done with a solution of ethanol and water (50% V/V) and the second and third with absolute ethanol. Finally, the nanoparticles were left drying overnight in a ventilated oven at 50°C.

2.3.2 MODIFICATION OF THE MSNS PORES

The external and internal surface of MSNs was modified by post synthetic method with organic alkosilanes containing functional groups with different polarity in order to test interactions between the functional groups and FNB. [43] 3-(Aminopropyl)triethoxysilane (APTES,) and Trimethoxy(phenyl)silane (TMPS) in Figure 10 ,were selected by its hydrophilic and hydrophobic characteristic respectively. Thus, TMPS, known to be a hydrophobic substance, was chosen to test a hydrophobic-hydrophobic interaction with FNB, while APTES, a hydrophilic substance, was chosen to test hydrophilic-hydrophobic interaction.

The functionalization reaction took place in nonpolar anhydrous solvents to avoid a reaction of the organosilanes with anything but the silica material. Organotrialkoxysilanes produce silanol groups by hydrolysis, which can be condensed with surface Si–OH group to form stable siloxane bond, Si–O–Si, for surface modification leading to an optimization of the drug absorption and achieving a slow-release effect to avoid the problem of drug burst release. [43] The modification of the nanoparticle surface with APTES (MSNs_APTES) schematic represented in Figure 11 was performed by suspending 0.166 g of MSNs in anhydrous toluene (10 mL) under an argon atmosphere into a 25 mL round bottom flask. This flask was sonicated under argon atmosphere for 15 min. Subsequently, APTES (0.10 mL) was added

dropwise and the resulting mixture was maintained at 130°C under reflux in an argon atmosphere for 24 h. Solid product (MSNs_APTES) was obtained by centrifugation at 1100 min^{-1} for 10 min and washed three times with absolute ethanol, discarding each time the supernatant. The particles were dried in a ventilated oven for 24 h at 50°C. The reaction mechanism is described in Figure 11.

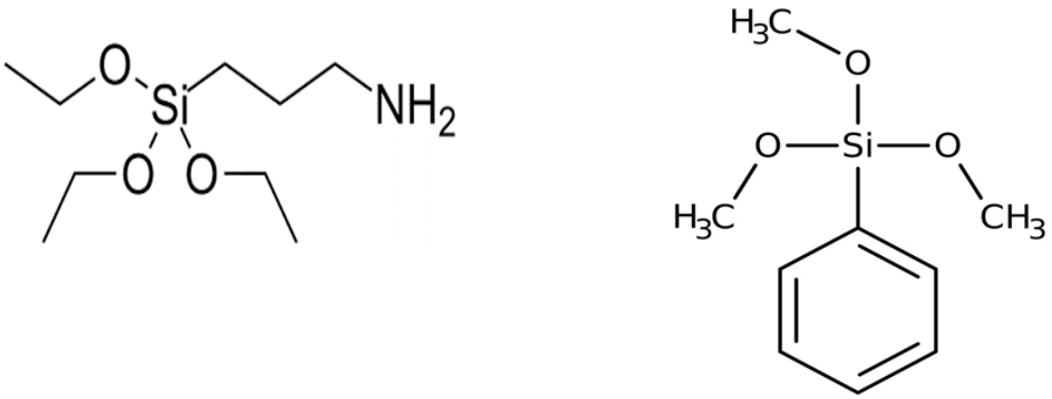

Figure 10. Chemical structure of 3-(aminopropyl)triethoxysilane (APTES) (left) and of trimethoxy(phenyl)silane (TMPS) (right).

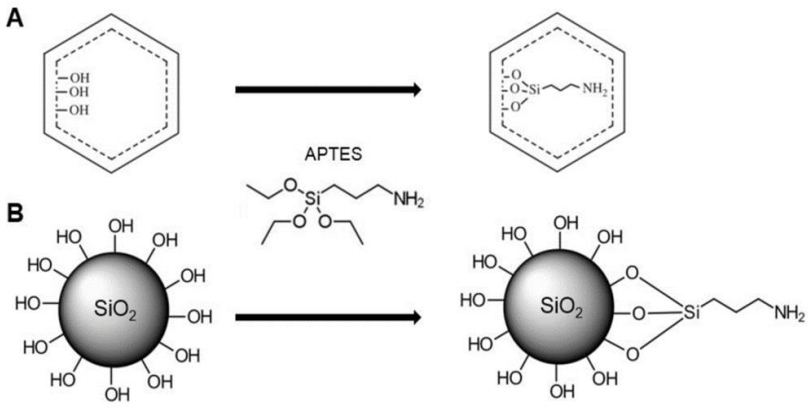

Figure 11. Amine internal (A) and external (B) surface functionalization with APTES molecule (adapted from [44])

The surface of the MSNs was also covalently modified with trimethoxy(phenyl)silane (Figure 12). For this purpose, 0.169 g of nanoparticles were dispersed in 15 mL of dry toluene.

Then, 50 μL of TMPS was added to the mixture and it was maintained at 125ºC under reflux with argon atmosphere for 24 h. The nanoparticles were recovered by centrifugation and washed three times with

ethanol (1100 min^{-1},10 minutes). After the last centrifugation the supernatant was removed, and the particles were dried overnight at 50ºC and MSNs_TMPS was obtained as solid product.

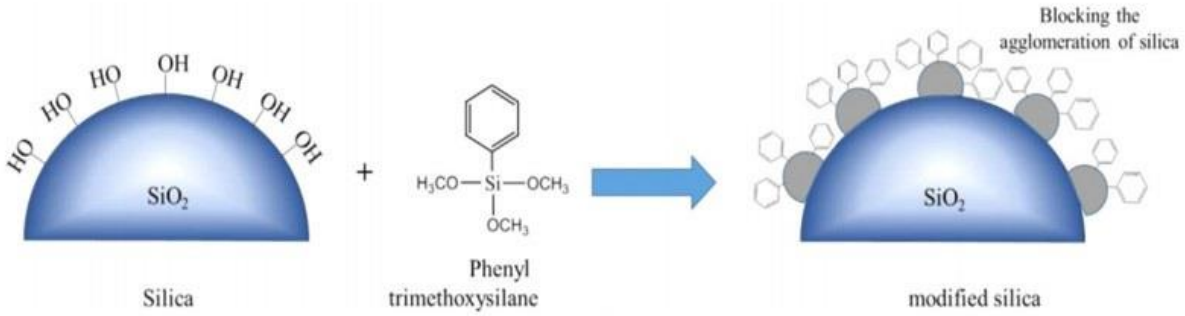

Figure 12. Schematic functionalization with TMPS molecule adapted from [45])

2.3.3 Fenofibrate Loading in Mesoporous Silica Nanoparticles

One of the main strengths of silica nanostructure materials is their use as drug delivery systems, mainly due to the high surface area and pore volume bring to a very high cargo capacity and controlled sustained release of the drug at the chosen localization, to achieve an increase in drug therapeutic efficacy and a reduction in side effects. There are two main strategies for drug loading, in situ during synthesis or as post-sorption (either by physisorption or by chemisorption). The loading step is usually performed as a separate step after the synthesis. This separation allows an optimization of the loading system (especially for poor soluble drugs) and physicochemical and structural properties of the carrier. [46] Drug loading was performed in solution under vacuum to eliminate water and other impurities, which could be contained in the pores of silica. Mesoporous nanoparticles were placed in a glass cell under vacuum (10^{-4} bar) and heated up to 150°C by immersion of the cell in an oil bath, for 8 h. After this period, the cell was allowed to cool down to room temperature and was kept under vacuum until use. Since fenofibrate has low solubility in water, it was dissolved in 2 mL of acetone to facilitate the process of loading into the silica matrix. The drug solution was then transferred to the glass cell containing the nanoparticles under vacuum and stirred for 3 hours to increase the uptake of Fenofibrate. Finally, the solvent was allowed to evaporate for one day under gentle stirring at room temperature without vacuum, after which a dry powder was obtained (FNB@MSNs).

2.3.4 Fenofibrate Loading in Mesoporous Silica Nanoparticles modified with Functional groups

The same procedure was repeated under the same conditions for the MSNs previous functionalized with either APTES or TMPS and a dry powder was obtained (FNB@MSNs_APTES or FNB@MSNs_TMPS). Table 1 presents the drug loading conditions for all the silica carriers.

The theoretical maximum of loading was estimated as [47]:

$$maximum\ loading = \left[\frac{V_p * \rho_{FEN}}{1g + V_p * \rho_{FEN}}\right] * 100\% \qquad \text{(Equation 1)}$$

Being ρ_{FNB} the density of fenofibrate (1.177 g/cm^3 taken from reference [48] for form I of crystalline FNB) and V_p the mesopore volume of the silica. The latter has been estimated from data obtained by BET analysis relative to similar mesoporous silicas nanoparticles described in reference [18] and has a value of 0.68 cm^3/g. The maximum theoretical load calculated from eq.1 is approximately 44 wt%. However, it must be noted that this value is overestimated given that the density of crystalline FNB is different to that of the amorphous form. [48] Also, it is linked only to the non-functionalized silica. In the modified ones the mesopore volume could decrease slightly due to the mesoporous channels being occupied by the modifying agent. Having this in mind, also the filling percentage (v/v) was estimated, taking in account the loading. Drug loading conditions are presented in Table 1.

For the mass of silica used, i.e. for 140.3 mg of bare MSNs, the pore volume available is calculated as: 0.1403 (g) * 0.68 (cm^3/g) = 0.095 cm^3. Being 0.0414 g the mass of FNB used in the loading of bare MSNs and 1.177 g/cm^3 the density of FNB, the volume of FNB is 0.035 cm^3.Considering the relation between MSNs pore volume and FNB volume, the maximum volume occupied will be around 37 vol% for unmodified silicas and silica modified with APTES (amount of drug loaded calculated as: mass of FNB/(mass of silica+mass of FNB)= 22.8 wt%). In the one functionalized with TMPS it will be higher, around 62 vol% (being the amount of drug loaded higher, 33.3 wt%).

Table 1. Drug loading conditions

Sample	Mass of silica (mg)	Mass of FNB (mg)	FNB loaded (wt%)	Available pore volume (cm^3)	Volume of crystalline FNB (cm^3)	FNB in silica pores (vol%)
MSNs	140.3	41.4	22.8	0.095	0.035	37
MSNs_APTES	142	42	22.8	0.096	0.036	37
MSNs_TMPS	120	60	33.3	0.081	0.050	62

3.RESULTS AND DISCUSSION

A novel control release system, consisting in a mesoporous silica MSNs functionalized with APTES or TMPS was synthesized. These compounds interact with the cargo molecules controlling the delivery rate.

3.1 MSNs SYNTHESIS AND CHARACTERIZATION

The morphological evaluation (size, shape and morphology) of the mesoporous nanoparticles was performed using transmission electron microscopy (TEM). In Figure 13 is represented one TEM image of the same sample in different scales and the respective diameter distribution. The mean diameter of the MSNs is (49 ± 6.6) nm. Mesoporous nanoparticles present smooth surface and spherical shape.

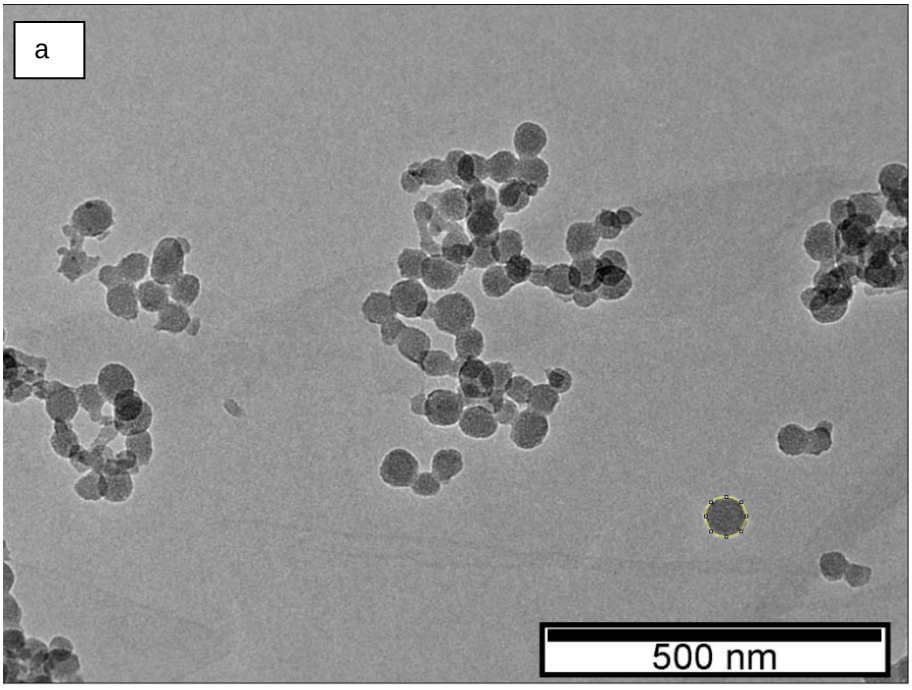

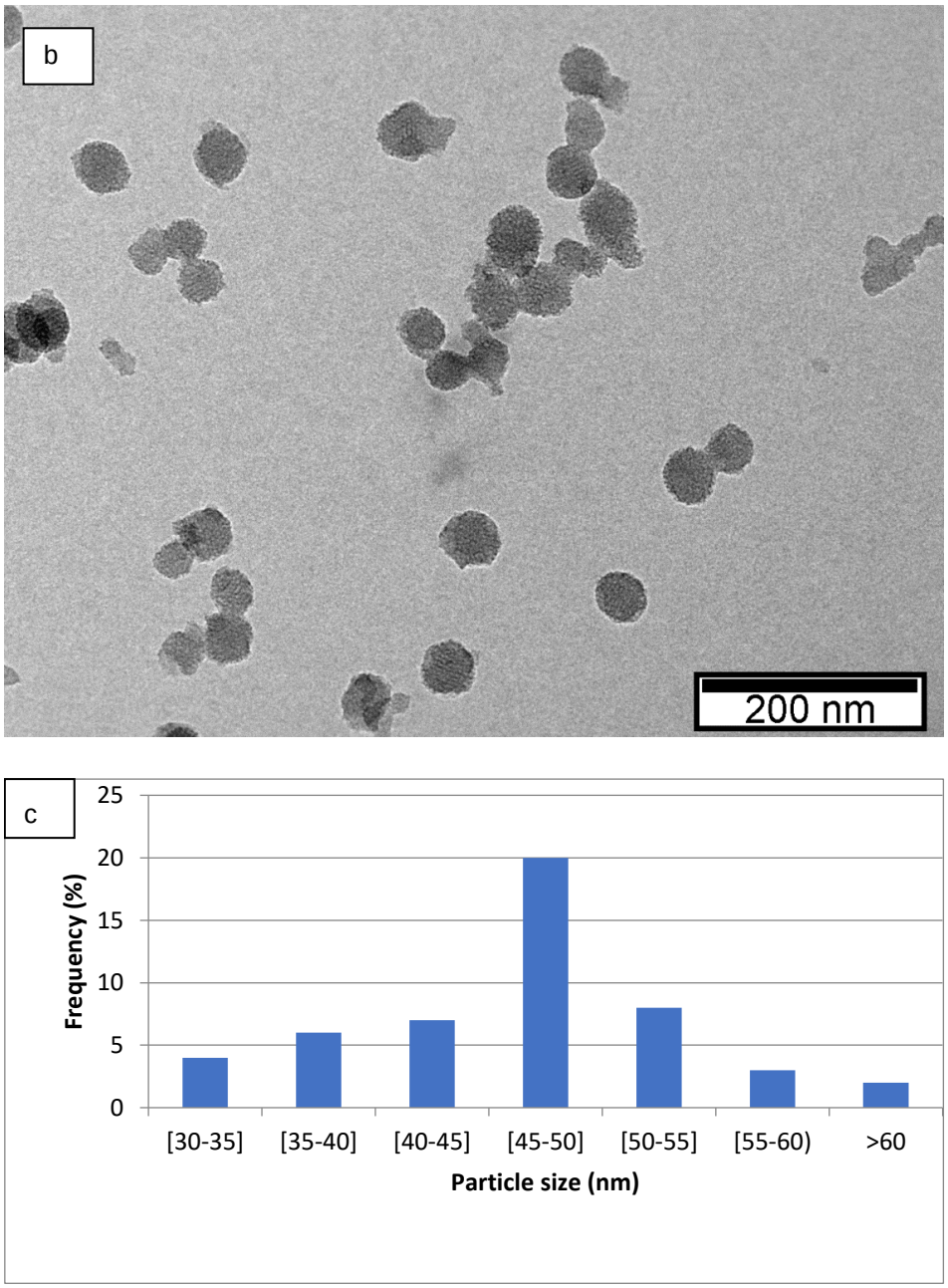

Figure 13 (a, b) TEM of the synthesized MSNs; (c) Histogram of the size distribution from the TEM data. The mean particle size is (49 ± 6.6) nm, based on 50 measurements.

3.2 FUNCTIONAL GROUPS

Surface functionalization can solve many of the applicability problems that are present in bare MSNs. Functionalization occurs through the reaction between organosilane molecules and the silica surface hydroxyl groups, both in the external particle surface and the interior pore wall surface. [54] In this work the functionalization was performed after template removal in order to obtained MSNs modified in both external surface and the internal (pore) surface, being the latter the one of interest. Specifically, the pore surface of MSNs was covalently modified with 3-(aminopropyl)triethoxysilane (APTES) and of trimethoxy(phenyl)silane (TMPS), two organic alkosylanes containing functional groups with different polarity. In particular, between a great diversity of surface functionalization options, amino functionalization has been shown to cause a significant increase in loading capacity of mesoporous drug host. [49] To confirm the integrity of the anchored organic molecules FTIR and NMR spectroscopy is most used.

3.2.1 IDENTIFICATION BY FTIR

The modification on the nanoparticle surface was confirmed by comparing the specific bands of the pure modifying agent with those observed in the functionalized silica. The FTIR spectra collected between 400 and 5000 cm^{-1} are presented in Figure 14 for pure modifying agent, bare MSNs and modified MSNs. Silica and modified silica samples have strong bands located at around 460 (δO-Si-O), 1100 (υ_{asym}. Si-O-Si), and 3300-3500 cm^{-1} (υSi-OH), confirming the presence of SiO_2 inorganic phase. [50,51].

The modified MSNs_APTES show two bands different from unmodified ones (see vertical dot lines in Figure 14)

(i) Around 2938 cm^{-1} attributed to C-N stretching vibration
(ii) At 1554 cm^{1}, related to N-H stretching vibrations of aminopropyl. [51]

These characteristics bands, observed in the FTIR spectra of MSNs_APTES but not in bare MSNs, confirm that the amino-propyl groups of APTES were successfully incorporated in the MSNs.

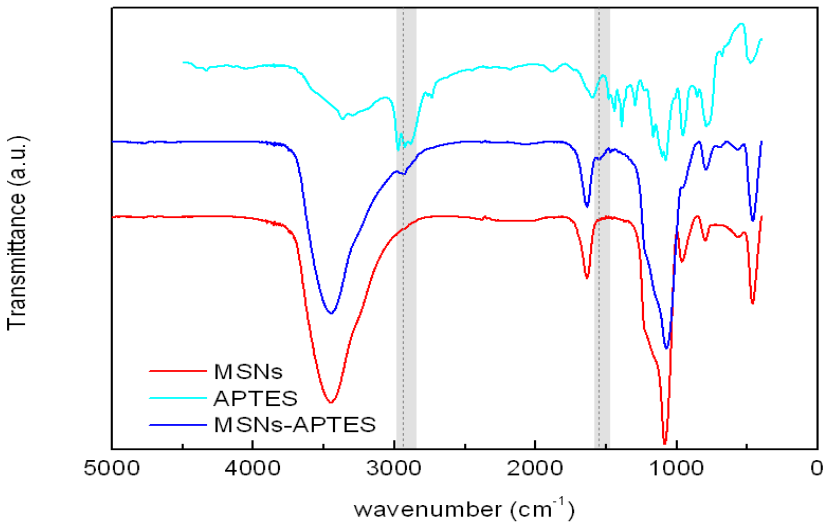

Figure 14. FTIR spectra of pure APTES, bare MSNs and modified MSNs_APTES

The silica functionalization with TMPS showed the following bands (grey regions in Figure 15):

(i) Between 2925 cm^{-1} and 2855 cm^{-1} attributed to methoxy groups [52]

(ii) At 1433 cm^{-1} attributed to Si-OCH_3 bond [53]

(iii) At 749 cm^{-1} and 700 cm^{-1} attributed to Ph-Si bond [53]

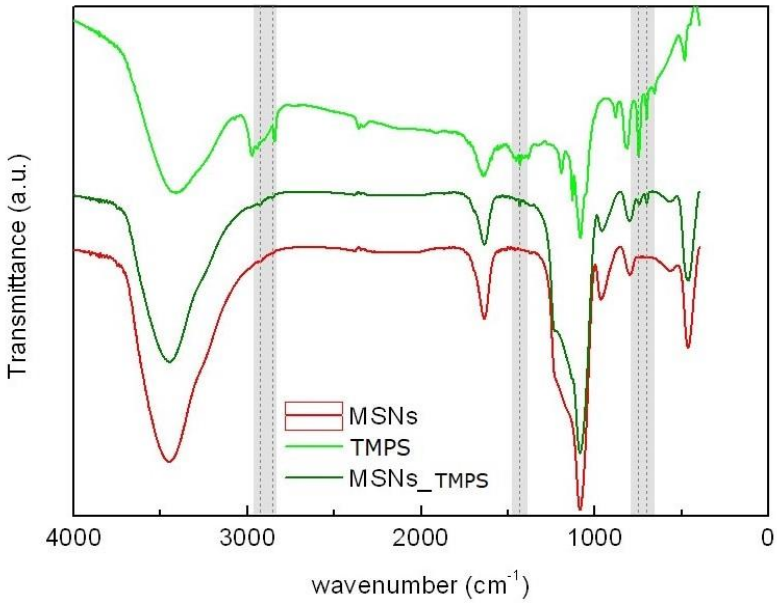

Figure 15. FTIR spectra of pure functionalized agent (TMPS), bare mesoporous nanoparticles (MSNs) and modified mesoporous nanoparticles (MSNs_TMPS).

Since the characteristic bands of MSNs_TMPS are barely observed in the FTIR spectra, suggest that TMPS modifying agent was not successfully incorporated in the MSNs. However, this technique is not

intrinsically surface-sensitive so a more accurate quantification and identification analysis should be done.

3.2.2 QUANTIFICATION BY NMR

Species anchored to nanoparticles have much lower mobility, and this bring to problems in their detection. To confirm the integrity of the anchored organic moieties a solution NMR was used to track silica surface modification and quantify functional group coverage. After dissolving the silica matrix in a mixture of two solutions (400 µL of a solution of NaOH and 100 µL of a solution of 1,3,5-trioxane), the ^{1}H-NMR spectra can be resolved for every single component of the mixture due to the improvement of the molecules mobility in solution. [54] In fact, organic molecules acquire the necessary mobility for NMR detection consequently to the in-situ destruction of the silica network at high Ph. All the peaks have been assigned and associated to specific atom positions in the structure. 1,3,5-trioxane was used as internal standard. In all the samples, the ethoxy group generates distinct resonance at 1.2 ppm and 3.6 ppm. These peaks correspond to resonances of residual ethanol from washing the MSNs after synthesis (solvent remain entrapped on the silica matrix after drying) and could denote a possible incomplete condensation of the alkoxysilane groups on the MSNs. Concerning MSNs_APTES compound The amount of the organic molecules grafted on the surface and inside the pores of the MSNs was estimated by comparing the integrated intensities of the peaks from the alpha- carbon to the silicon atom (less affected by possible interactions of the functional group) with the intensity of the internal standard. [54] In Figure 16 is presented the ^{1}H NMR spectra for silica nanoparticles functionalized with APTES.

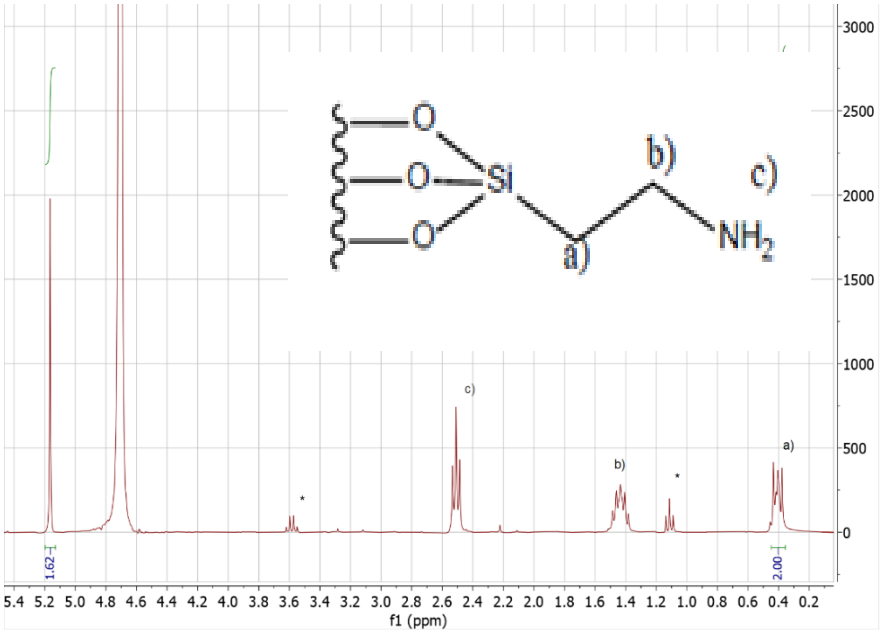

Figure 16. ^{1}H NMR spectra recorded of MSNs_APTES in NaOH/D_2O.The internal standard peak is at 5.15 ppm. Ethanol peaks are marked with (*).

^{1}H NMR (D_2O): 0.38 ppm (t, 2H, Si-CH_2-); 1.41 ppm (q, 2H, -CH_2-); 2.49 ppm (t, 2H, -NH_2); 1.09 ppm (solvent, C**H**$_3$$CH_2OH$); 3.57 ppm (solvent, CH_3C**H**$_2$OH); 4.71 ppm (D_2O); 5.15 ppm (internal standard, C_3**H**$_6O_3$). [54]

The integrated intensity of the peaks from the alpha-carbon (δ=0.38 ppm) was normalized to account the two protons bond to it. Then the molar amount of APTES was calculated by knowing the molar amount of the IS and using the value for the integrated intensity of the internal standard peak (I_{IS}) previously divided by the numbers of protons of 1,3,5-trioxane (6 protons).

$$n_{APTES} = n_{IS}/I_{IS}$$

The surface coverage (molecules per nm^2) was calculated from the surface area and volume of a particle and a density of 0.34 g/mL [54] was used for the mesoporous nanoparticles. First, from the mean particle size we calculated the area ($A = 4\pi r^2$) and volume ($V = 4/3\pi\ r^3$) of the particles. The mass of a particle was calculated from the density and the calculated volume, allowing the quantification of the number of particles per gram of material. With the number of particles per gram and the area of an individual particle, we determined the total area (m^2) per gram. The concentration of the functionalized compound (mol/m^2) can then be obtained from the total area and the value obtained by NMR (mol/g). From this the corresponding number of molecules/nm^2 is obtained. For example, the amine concentration, determined by ^{1}H NMR was 3.14 mmol/g, corresponding to a surface density of 1.93 amine groups per nm^2. Same procedure and calculations were kept for quantify the modifying agent TMPS in the nanoparticles as reported in Figure 17.

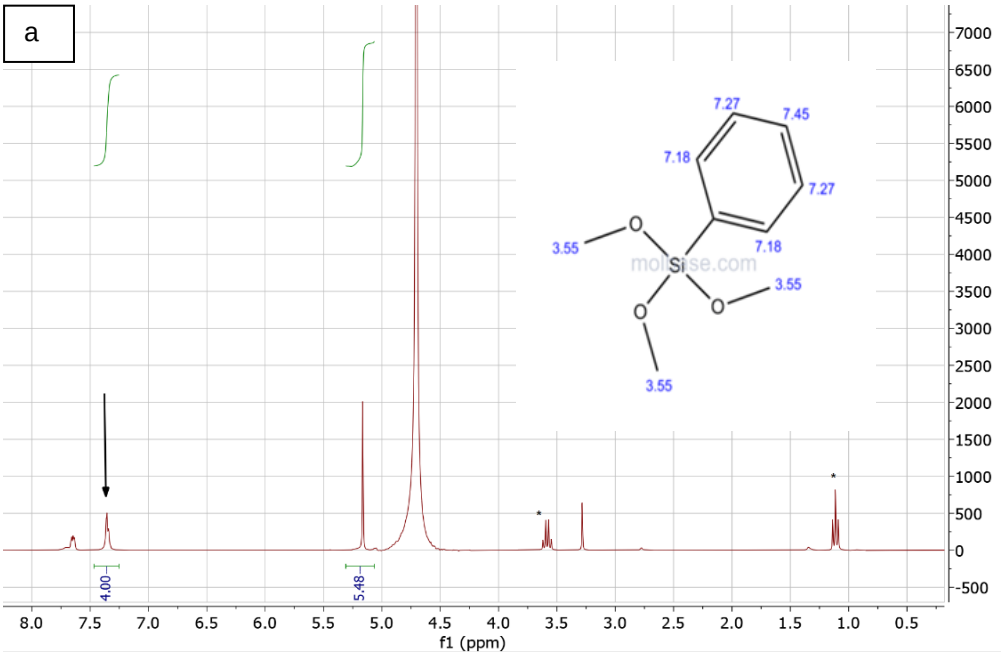

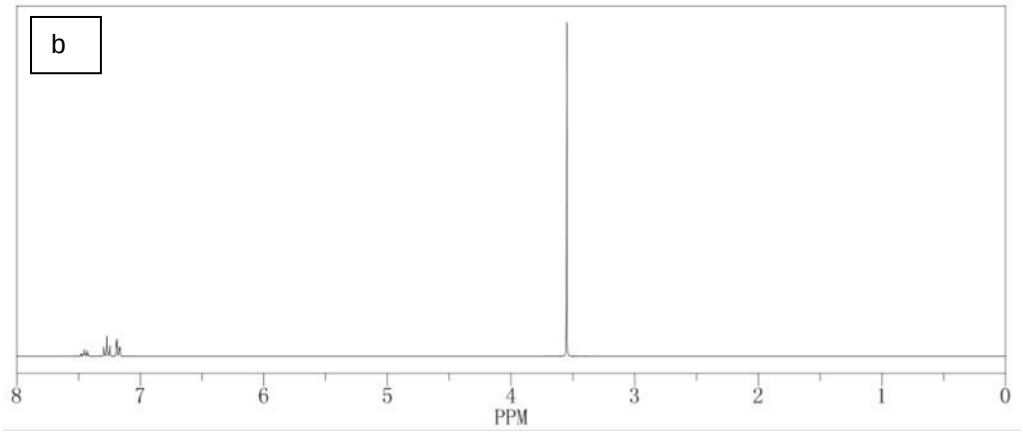

Figure 17. ^{1}H NMR spectra recorded at 400 MHz of MSNs_TMPS in NaOH/D_2O. The internal standard peak is at 5.15 ppm. Ethanol peaks are marked with (*) (a). ^{1}H NMR spectra recorded for pure TMPS from the database (b) (guidechem.com).

The peaks between 7.3 and 7.4 ppm have been assigned to the presence of TMPS and associated to the hydrogen positions at 7.18 and 7.27 in the aromatic ring. The shift is produced since in the sample analyzed not only TMPS is present. The integrate intensity of the peaks from the aromatic ring was normalized to account the four protons bond to it. This normalization was stabilized because peaks were found grouped in the sample and thus associated to hydrogen positions at 7.18 and 7.27 ppm.

Assuming that the three alkoxide groups in an organosilane molecules could covalently react with up to three Si-OH sites, the maximum number of functional groups that can be anchored in the MSNs should be in the range of 1~3 molecules/nm^2. The values obtained by solution ^{1}H-NMR related to the anchoring of APTES molecules are in good agreement with this upper limit, showing good control of the surface modification procedure. However, nanoparticles functionalized with TMPS present less modifying agent anchored on the silica matrix. In Table 2 is presented the concentration of APTES and TMPS on the total surface of the nanoparticles.

Table 2. APTES and TMPS concentration on the MSNs, calculated by ^{1}H NMR

Sample	mmol/g MSNs	Modifying agent molecules/nm^2
MSNs_APTES	3.14	1.93
MSNs_TMPS	0.98	0.60

3.3 FENOFIBRATE LOADED MSNs

Before loading the MSNs, these were dried at 150ºC during 8 h under vacuum; after that, they were cooled naturally down to room temperature. A solution of FNB in 2 mL of acetone was injected in the MSNs container. After drying overnight at ambient temperature, a final product was obtained as powder.

3.3.1 IDENTIFICATION BY FTIR

FTIR was used to evaluate if successful loading of fenofibrate was achieve by comparing the specific bands of the native drug with those observed in the loaded silica. Moreover, a possible interaction between functional or silanol groups with the drug is evaluated. In Figure 18 are represented the FTIR spectra of all the samples under study.

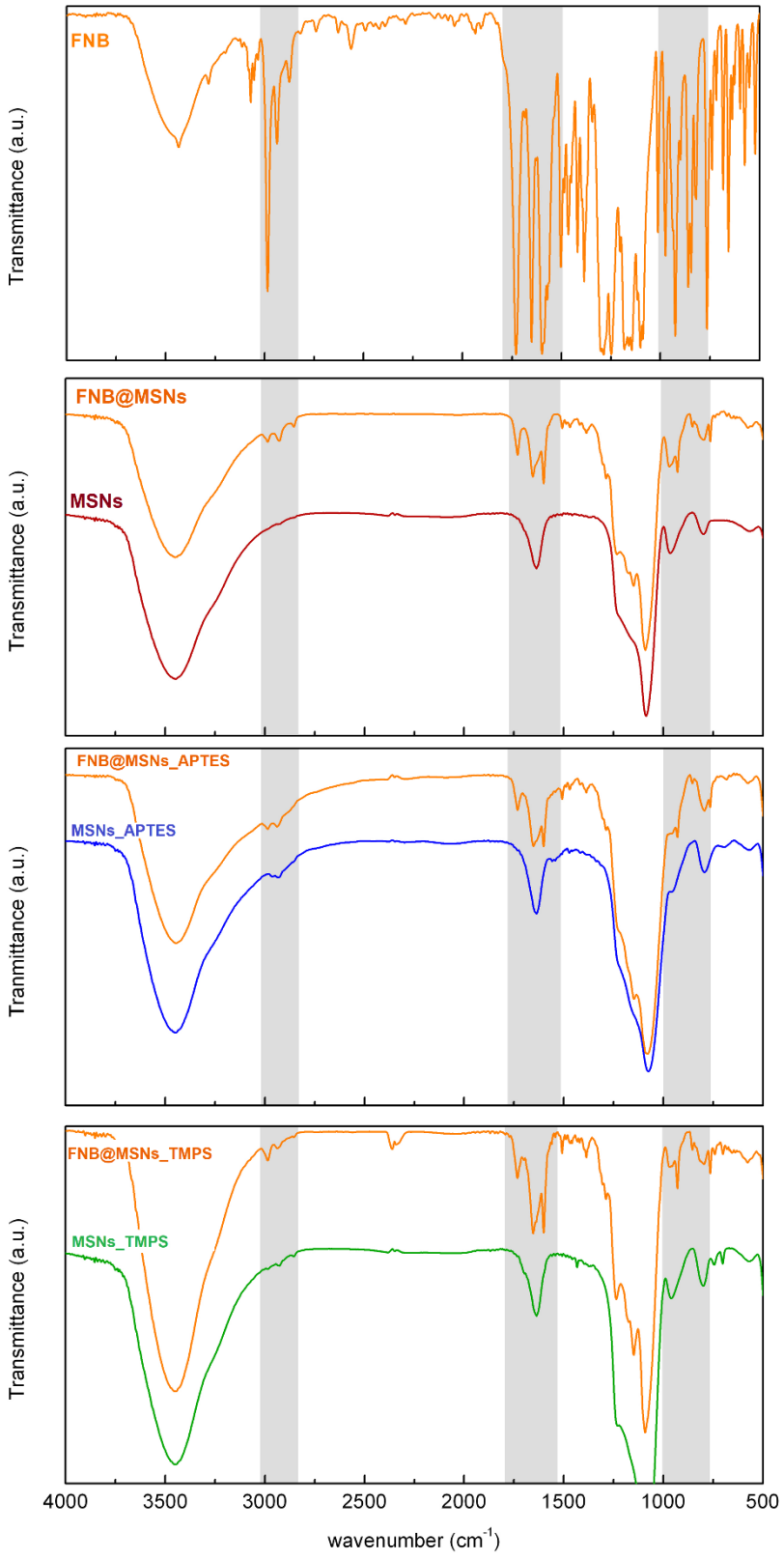

Figure 18. FTIR spectra obtained for three MSNs, unmodified, functionalized with APTES and functionalized with TMPS, without and with fenofibrate. Grey rectangles identified the principal regions of FNB bands.

In a general way, the presence of FNB in the loaded nanoparticles is noted by the several and small intense bands superimposed to the unloaded matrixes. From a more detailed comparison between three composites with fenofibrate the more relevant changes are:

- in the region around 3000 cm^{-1} where FNB bands assigned to the CH stretching of isopropyl group [55, 56] are visible in three systems, even with the superposition of APTES bands in FNB@MSNs_APTES sample.
- A strong band between 1750 and 1550 cm^{-1} assigned to C=O stretching [55] is observed in three samples (Figure 18). At 1728 cm^{-1} and 1650 cm^{-1} two sharp bands are detected in pure crystalline FNB assigned to stretching vibrations of carbonyl in the ester group and to the carbonyl in the ether group between benzene rings respectively. [57] Both are also observed in FNB loaded in MSNs and while the first one continues well-defined, the latter is overlapped to a broad band present in unloaded silicas. The position is slightly shifted to higher wavenumbers in FNB loaded systems, which has been taken as an indication of a more disordered phase as it is the case of amorphous versus crystalline state.
- Between 1598 and 1570 cm^{-1}, multiple peaks arise partially overlapped in pure FNB which have been assigned to in-plane benzene stretch and benzene ring deformation [57]. When FNB is loaded in mesoporous matrixes, only a very well-defined band is observed in this region, centered at 1600 cm^{-1} (figure 19). This may indicate that only one of the vibration modes, that corresponding to in-plane benzene ring stretch [57] (intermediate ring), is allowed when FNB is loaded in MSNs. A possible explanation for this effect can be related to the hydrogen bonds formed between FNB and silica. In this sense, it must be noted that FNB can't form hydrogen bonds to other FNB molecules due to the lack of hydrogen-bond donating groups [57]. The disappearance of some of vibration modes could be due precisely to the formation of strong H-bonds between FNB and silica that favor one of the possible stretch vibrations in detriment of the others. In term of conformations, it could be possible that the external ring is parallel to silica surface while the intermediate ring assumed a perpendicular position.
- Between 1000 and 700 cm^{-1}, small peaks are visible in the three MSNs with similar intensities in MSNs and MSNs_APTES and only that at 928 cm^{-1} is clearly less intense in MSNs_TMPS. The reduced intensity of this band in the last sample (which has higher FNB loading), could suggest more restricted vibrations related to C-C-H in plane deformation .[55]

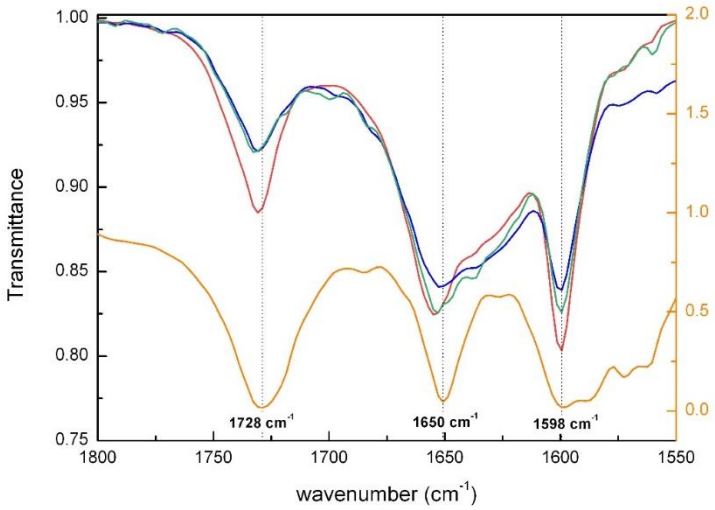

Figure 19. FTIR spectra of bulk FNB (orange) FNB@MSNs (red), FNB@MSNs_APTES (blue) and FNB@MSNs_TMPS (green) in the carbonyl stretching region.

*3.*3.2 QUANTIFICATION BY NMR

Various NMR experiments were performed to obtain information on the fenofibrate incorporation on MSNs. However, it was not possible to clearly quantify the amount of fenofibrate on the MSNs due to impurities present in the sample and solubility problem. In fact, the complete dissolution inside the tubes was not achieve, even after addition of d6_DMSO. These two factors lead to an error in the estimation of drug quantity. Figure 20 shows an example of ^{1}H NMR spectra of fenofibrate incorporated in unfunctionalized silica nanoparticles. Peaks around 1.32 ppm were recognized the most characteristic signals of fenofibrate and associated to the hydrogens of the isopropyl group. However, in the same region the peaks of residual ethanol from the washing are also presents, thus, it is not possible to clearly attribute the peaks observed to only the native drug and an overestimation of the drug incorporation in the loading of bare and functionalized nanoparticle is expected.

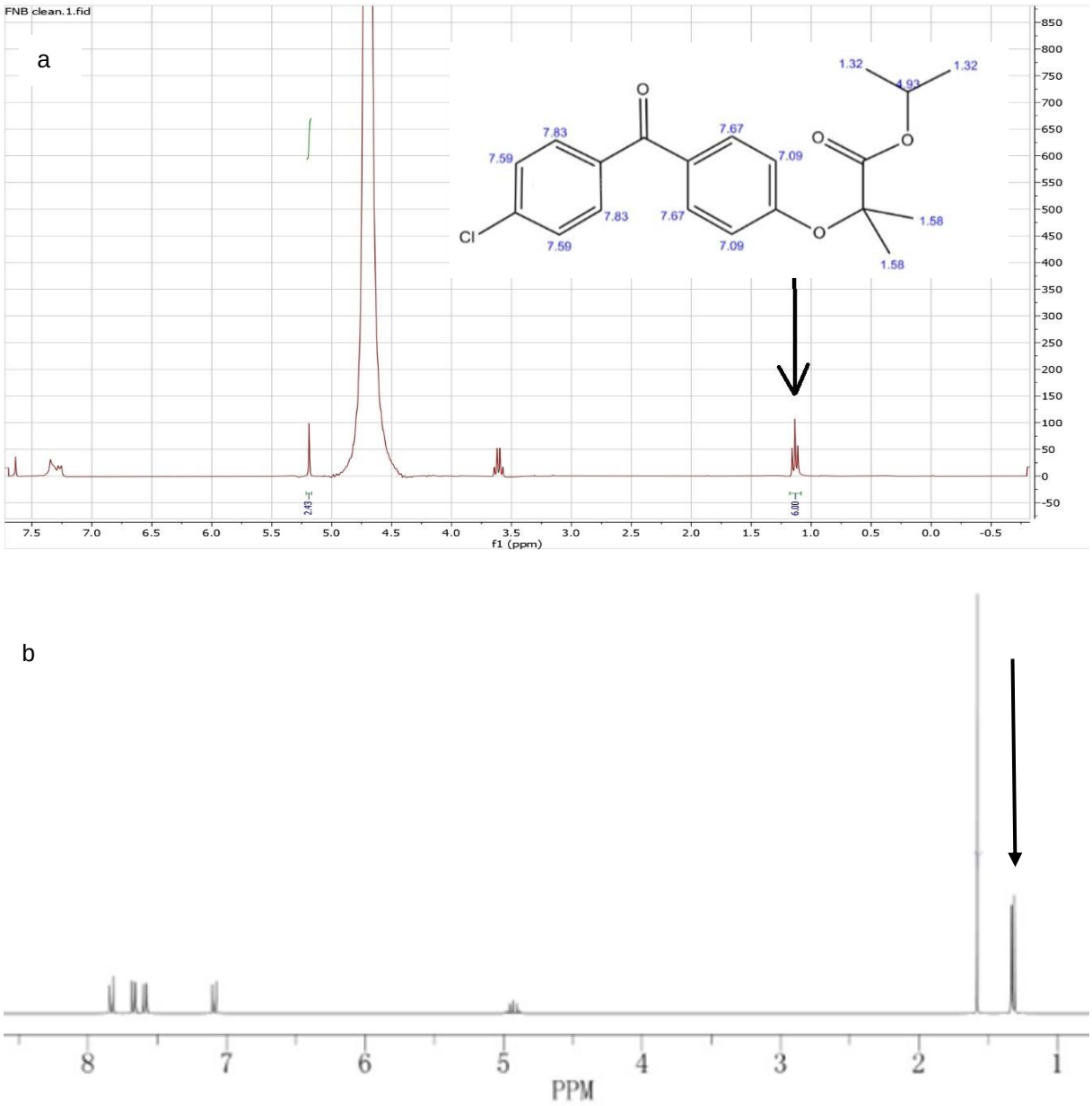

Figure 20. ^{1}H NMR spectra of FNB@MSNs in $NaOH/D_2O$. The internal standard peak is at 5.15 ppm. The arrow indicates the considerate peaks (a). ^{1}H NMR of pure FNB from literature (b) (guidechem.com).

In order to try to overcome this problem of attribution, peaks around 7-8 ppm where took in consideration (Figure 21), as they also appear in the database for the native drug. These peaks correspond to resonance of the hydrogens in the aromatic rings of the molecule specifically at 7.59 ppm and 7.67 ppm. Thus, these peaks were normalized to count the 4 protons bond to it. However, the comparison with the internal standard peak leads to a molar amount of fenofibrate that exceed the molar amount of FNB that was incorporated in the silica matrix, possibly due to the presence of some impurities that produce resonance in the same region and lead to an incorrect and overestimated value of moles present in the silicas.

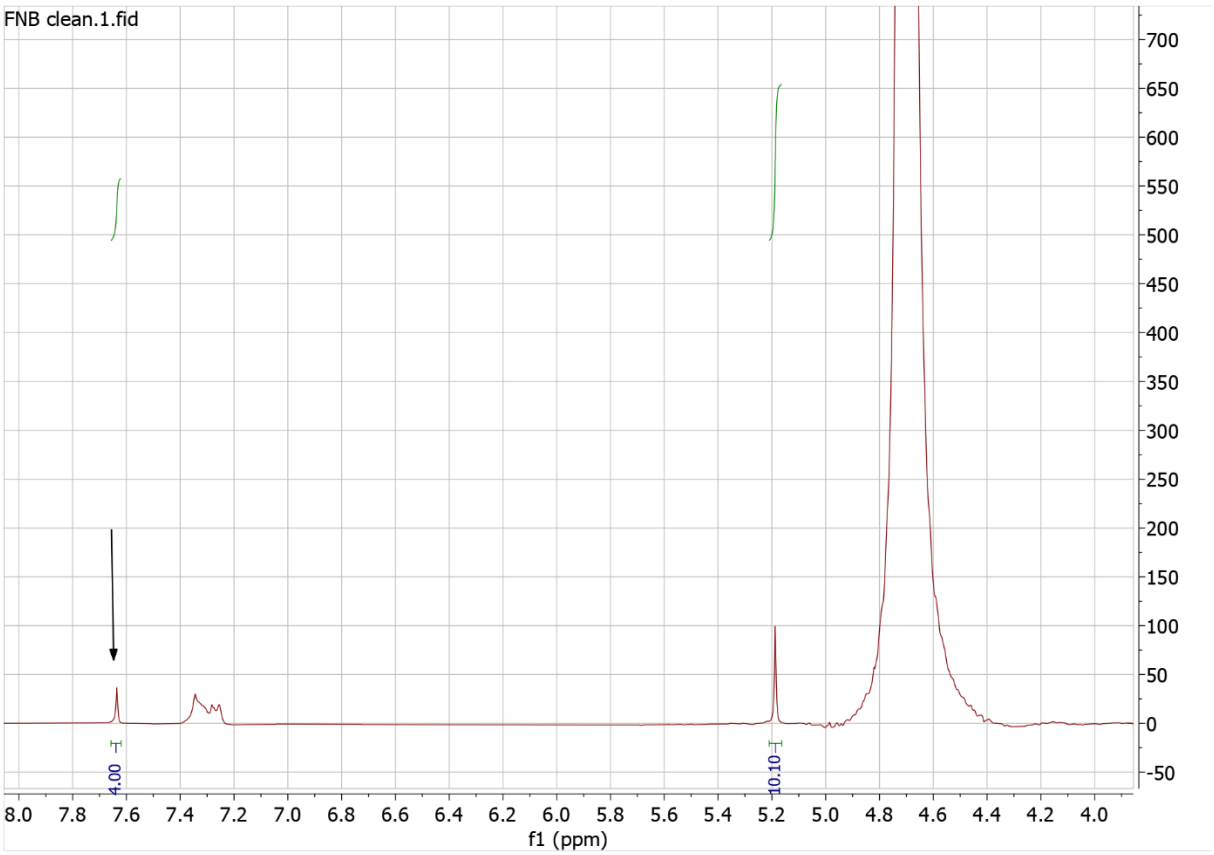

Figure 21. ^{1}H NMR spectra of FNB@MSNs in $NaOH/D_2O$. The internal standard peak is at 5.15 ppm. The arrow indicates the evaluated peaks at higher ppm regions (around 7.6 ppm).

3.3.3 Quantification by UV-Vis

The characterization of small molecules immobilized on the pore surface of MSNs is a very challenging task. As it is reported above, FTIR spectroscopy can be used to identify functional groups on the surface of MSNs. However, this technique is not quantitative and not intrinsically surface-sensitive regarding the inner core of MSNs. [54] On the other hand, NMR spectroscopy provides quantitative information on the surface modification of MSNs. However, could not be used due to the possible contamination of signals as it happened in the quantification of FNB inside the silica matrixes. Thus, the supernatants of the nanoparticles, that were previously centrifugated and cleaned, were saved, weighted and used to determine the loading efficiency, by UV-Vis absorption spectroscopy. In Figure 22 are presented the absorption spectra of the supernatants of FNB@MSNs_APTES in EtOH.

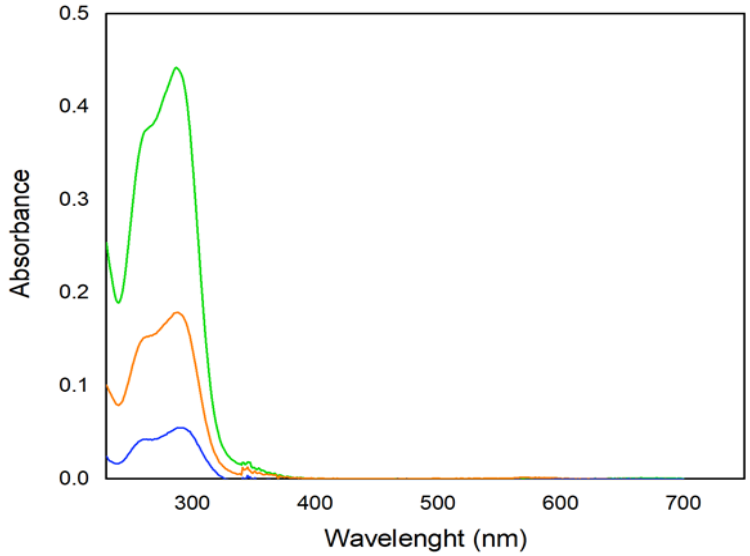

Figure 22. Absorption spectra of the diluted supernatants recovered after centrifugation of FNB@MSNs_APTES in EtOH. Supernatant 1 removed after the 1st centrifugation (green), supernatant 2 removed after the 2nd centrifugation (orange) and supernatant 3 removed after the 3rd centrifugation (blue).

To estimate the concentration and then the number of moles of FNB in each supernatant it was constructed a calibration line. The calibration curve is presented in Figure 23 and its equation is $A = (16.7 \pm 0.8)x10^3 x\, C + (0.0064 \pm 0.0003)$ where the slope represents $\boldsymbol{\varepsilon}$ (molar absorptivity coefficient) and C is the concentration.

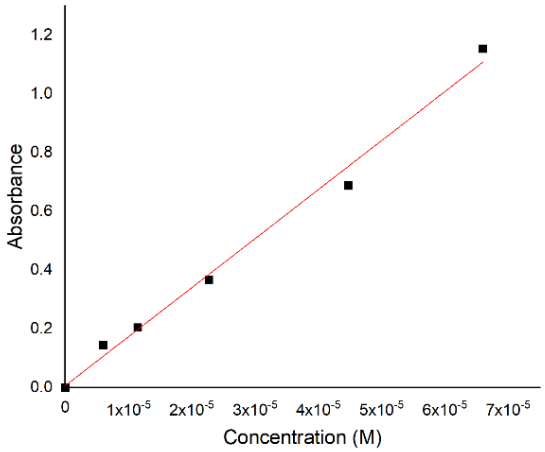

Figure 23. Calibration curve of FNB solutions in EtOH

By using the value of the absorbance at λ= 259 nm and the calibration curve of FNB (mother solution of FNB in EtOH), the number of moles of FNB in each supernatant was determined (Table 3). Afterwards the amount of incorporated FNB in bare and functionalized nanoparticles was obtained by subtract the

sum of the quantities present in each supernatant to the initial quantity of FNB moles that were previously washed (Table 4).

Table 3- number of moles of FNB in the supernatants for each sample.

sample	Supernatant 1 (mol)	Supernatant 2 (mol)	Supernatant 3 (mol)
FNB@MSNs	1.89×10^{-5}	1.58×10^{-5}	1.49×10^{-6}
FNB@MSNs_APTES	6.29×10^{-6}	9.69×10^{-7}	4.91×10^{-8}
FNB@MSNs_TMPS	2.32×10^{-6}	2.15×10^{-6}	1.68×10^{-7}

Table 4. FNB loading in the nanoparticles.

Sample	Amount MSNs (g)[a]	$n_{FNB\ add}$ (mol)[b]	$n_{supernatants}$ (mol) [c]	n_{MSNs} (mmol/g) [d]
FNB@MSNs	0.0937	5.92×10^{-5}	3.63×10^{-5}	0.245
FNB@MSNs_APTES	0.0244	1.54×10^{-5}	7.31×10^{-6}	0.332
FNB@MSNs_TMPS	0.024	2.21×10^{-5}	4.64×10^{-6}	0.729

[a] mass of MSNs washed with EtOH, [b] number of FNB moles in the washed MSNs, [c] number of FNB moles in the supernatants, [d] millimoles of FNB per gram of nanoparticles.

Table 4 shows that the number of moles of FNB incorporated are higher in the functionalized nanoparticles. Especially, it is observed a huge difference, from 0.245 mmol/g of FNB incorporated in bare MSNs up to 0.729 mmol/g in the amount of FNB incorporated after surface functionalization with the modifying agent TMPS. The high loading capacity of FNB into these silicas might be attributed to stronger interactions between the drug and TMPS (although a higher amount of FNB was used in the loading process in the MSNs_TMPS, a lower amount was detected in the supernatants). MSNs_APTES also presents a higher capacity to retain FNB, compare to the bare MSNs. Thus, since the mesoporous silica nanoparticles have the same size and morphology, the functionalities at the surface strongly affect the drug loading capacity.

3.4 PHYSICAL STATE OF FNB IN THE MSNs

To access the physical state of fenofibrate inside the silica matrix, differential scanning calorimetry (DSC) was used. Dielectric relaxation spectroscopy (DRS) was used to probe the molecular mobility of the drug. The different techniques provided complementary information and reveal that drug incorporation inside a nano porous matrix is a suitable strategy to stabilize fenofibrate in the amorphous state.

3.4.1 DSC RESULTS

Differential scanning calorimetry was used to study phase transformations of fenofibrate and fenofibrate in bare MSNs, MSNs_APTES and MSNs_TMPS. Thermogram of bulk fenofibrate as received is shown in Figure 24. On heating, FNB melt at 81 ºC (dotted line) with an enthalpy of 32.4 kJ/mol. On cooling after melting (red line), crystallization is avoided, and it enters in the supercooled liquid state. Around -17 ºC the signal of the glass transition is observed also in very good agreement with the value obtained. [58]

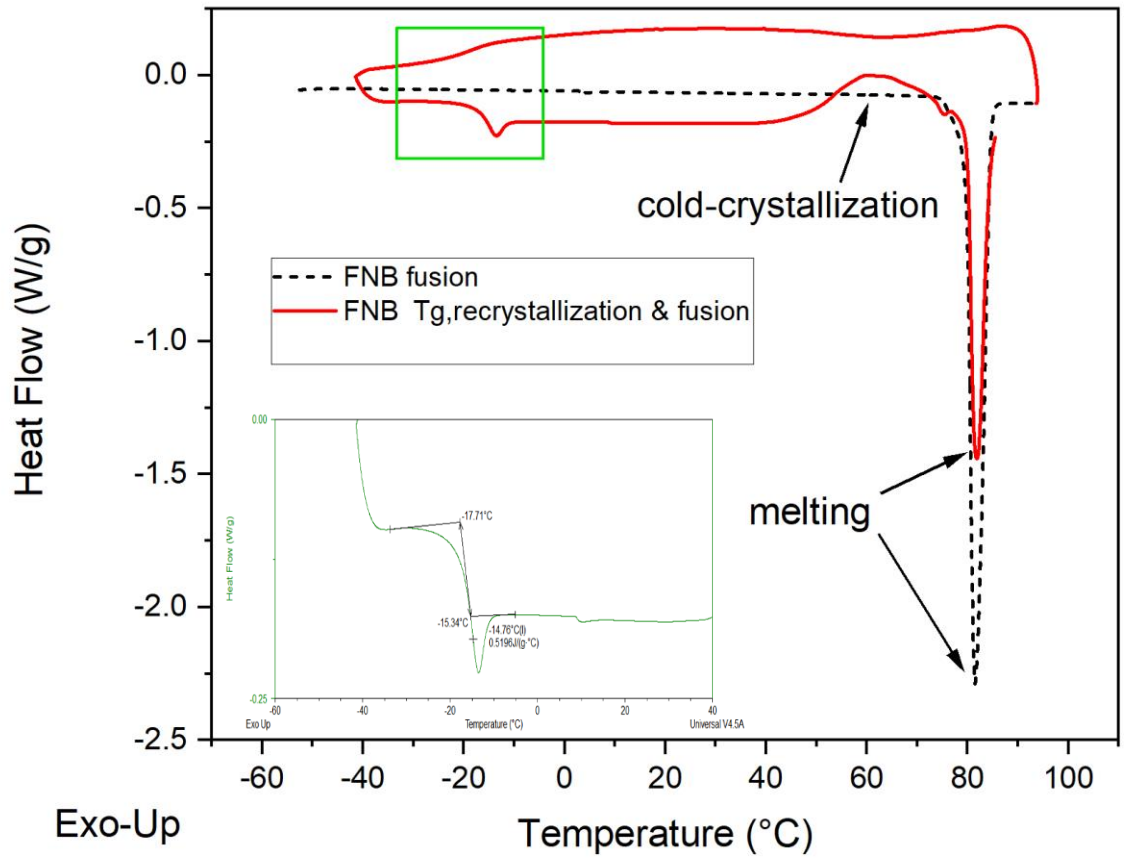

Figure 24. Thermograms of fenofibrate obtained at 10 ºC/min: dotted line, on heating from room temperature up to 95 ºC; red line, upon cooling down to -50ºC and then heating up to 90°C. Green square indicates the glass transition region that it is enlarged in the inset (heating) showing the auxiliary lines (dotted) used to determine the onset, midpoint and end set of this transition.[i]

In the subsequent heating, the glass transition temperature can be well defined at -17.71ºC ($T_{g\text{-onset}}$). Additionally during the second heating a broad exothermic peak was observed which revealed crystallization from the amorphous phase (T_{max} = 63 ºC). The corresponding melting is found at 81 ºC.

[i] Data provided by prof. Hermínio Diogo. [38]

Given that the temperature is equal to that obtained for the native sample, it can be assumed that the same crystalline and more stable form was originated. The enthalpy of 22.87 J/g indicates that only a fraction of the sample was recrystallized ($\Delta H_{cold\text{-}cryst}/\Delta H_{initial}$ *100 = 25.4 % crystallinity). This indicates that although fenofibrate is a good glass former it has tendency to recrystallize to its stable and structurally ordered crystalline state. Thus, fenofibrate was incorporated into mesoporous matrices with the aim to stabilize the compound in its amorphous form and thus improve its solubility, which may enhance bioavailability.

The study proceeds with the analysis of the physical state of fenofibrate inside nanoparticles. FNB loaded MSNs sample was submitted to two cooling/heating cycles between -90 and 120 °C. In the first heating a broad peak with minimum around 75°C is observed (blue line in Figure 25) caused by the water evaporation from the sample, since silica readily adsorbs water during manipulation. There is no evidence of the melting peak of fenofibrate, indicating that FNB is in the amorphous state inside the silica. Also, there is no evidence of thermal events during the second cycle meaning that fenofibrate converts to the amorphous form when is located inside the silica carrier and conversion in its crystalline form is avoided. However, it is not clear if the signal of the glass transition exists in the first heating scan (see square Figure 25).

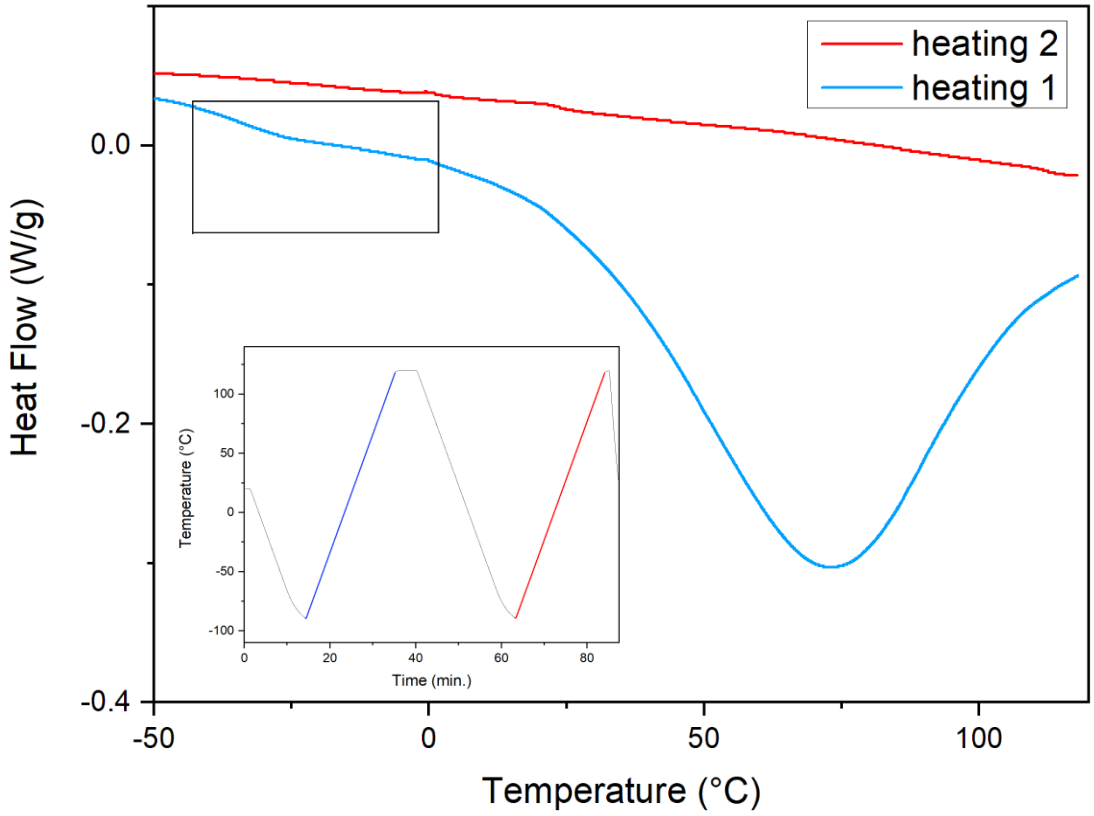

Figure 25. Heating thermograms at 10 ºC/min of FNB@MSNs. Inset represents the temperature/time experimental procedure followed.

To clarify this subject, a new fresh sample was analyzed following a gradual drying treatment consisting in successive cooling/heating cycles with increasing final temperatures (see right inset in Figure 26). The resulting heating scans are represented in Figure 26 where the step associated to the glass transition is clearly observed in the first heating as well as a shift to higher temperatures join to a reduction in the ΔC_p as the water is progressively removed. The values estimated for the glass transition temperature are summarized in Table 5 and put in evidence the plastificant effect of water in the T_g of fenofibrate since T_g found is always lower than that observed for bulk Amorphous FNB. It is also noticeable that a decrease of the water content leads to a decrease in the ΔC_p that is not only due to the reduction in the mass sample but also suggesting the strength of interactions between FNB and silica matrix. Additionally, it must be mentioned that the temperature range, in which the material undergoes a second order phase transition (i.e., liquid to glass or vice versa), is larger respect to the one in native fenofibrate because of the interaction with the silica.

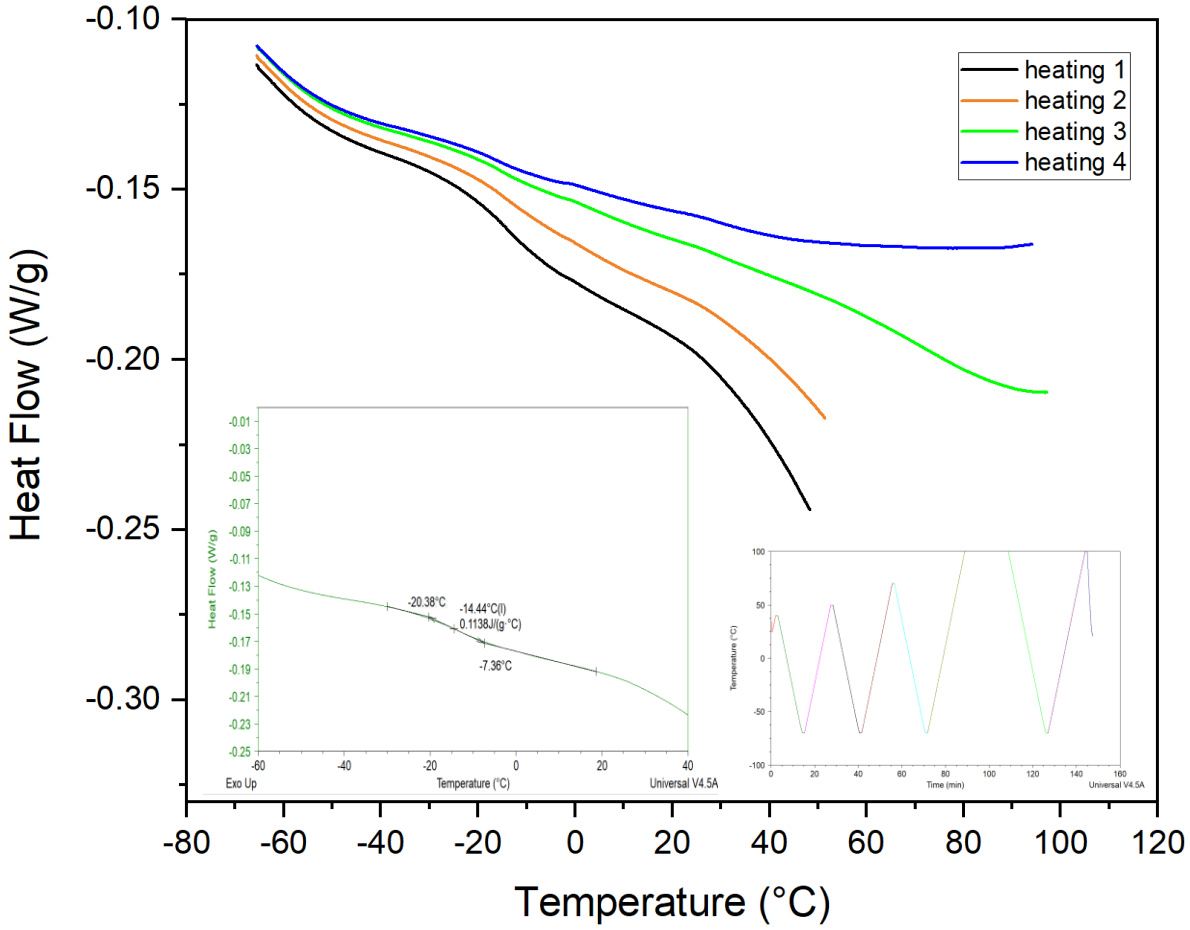

Figure 26. Heating thermograms at 10 ºC/min of the sample FNB@MSNs obtained with gradual heating. Left inset shows the enlarged glass transition range in the heating 1; Right inset represents the temperature/time experimental procedure followed. The final temperature of each cycle is: T_{f1}=50°C; T_{f2}=70°C; T_{f3}=100°C; T_{f4}=100°C.

Table 5. Glass transition temperature at the onset, midpoint and endpoint obtained on successive heating of the sample FNB@MSNs during the gradual drying treatment and respective heat capacity.

	$T_{g\text{-}on}$ (ºC)	$T_{g\text{-}mid}$ (ºC)	$T_{g\text{-}end}$ (ºC)	ΔC_p (J/gºC)
After T = 50 ºC	-23.64	-14.44	-7.36	0.1138
After T = 70 ºC	-22.68	-14.86	-5.57	0.1061

Regarding FNB@MSNs_APTES in the first controlled heating cycle up to 120°C the broad peak associated with the water release is overlapped by a less pronunciated endothermic peak at 80 °C associated with the melting temperature of fenofibrate revealing a small presence of crystallites in the sample (see Figure 27).

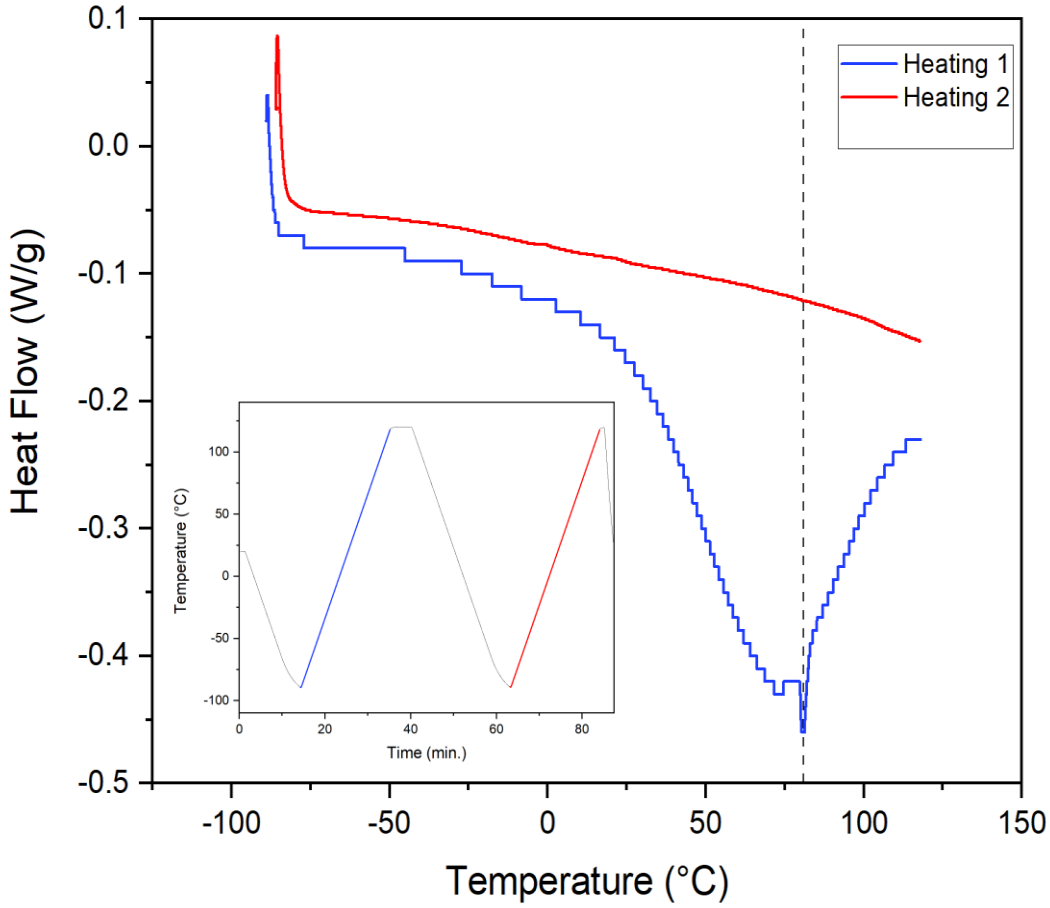

Figure 27. Heating thermograms at 10 ºC/min of FNB@MSNs_APTES. Inset represents the temperature/time experimental procedure followed.

Also, for this sample a gradual drying was performed in order to visualize better the interval of the glass transition temperature. In Figure 28 the heating scans are plotted and it is possible to observe as the endset is not well defined because the heat flow line in this region shows the initial water removal that was present in higher amount respect to the water content in bare nanoparticles. In fact, the shift of the T_g values observed in this sample relatively to that of fenofibrate incorporated inside bare MSNs is larger in the first heating (see values in Table 6). In brief, MSNs_APTES retain a large amount of water that act as plastificant and bring the T_g to lower values. However, it was not possible to establish values of T_g after temperature of 70°C due to the very low heat capacity change.

On the other hand, it must be noted that crystallization of FNB is not detected in this sample. It could be due to no homogeneity of the sample prepared or more probably it occurs during the water release or in the isothermal step between heating and cooling. In any case, it can be assumed that the crystalline fraction must be nearly insignificant versus that amorphous one.

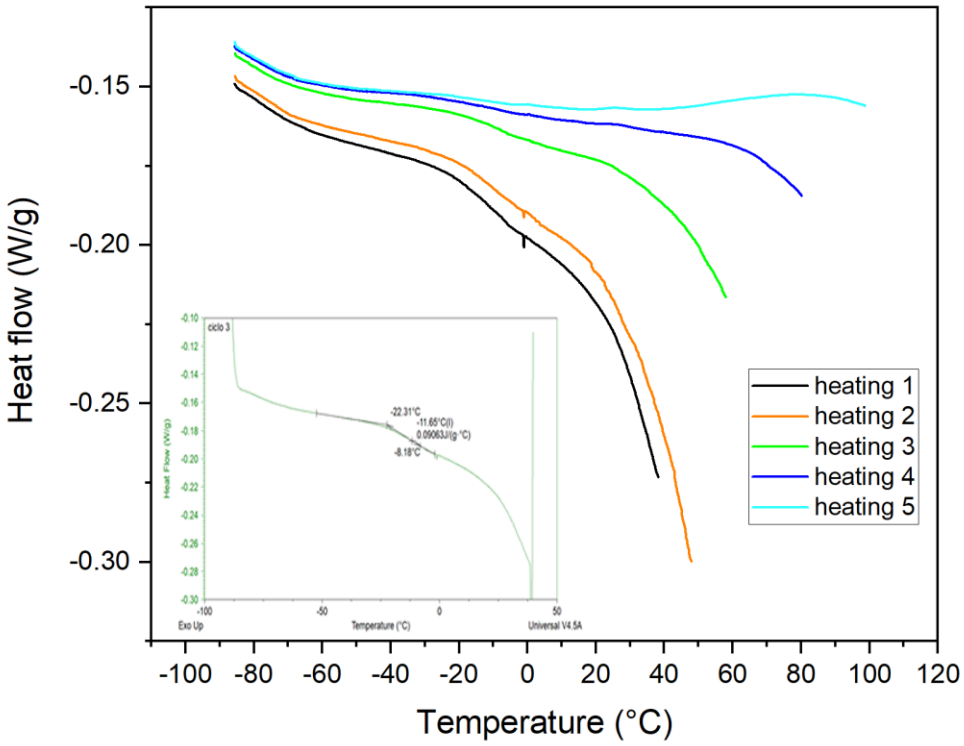

Figure 28. Heating thermograms at 10 ºC/min of the sample FNB@MSNs_APTES obtained with gradual heating. Left inset shows the enlarged glass transition range in the heating 1. The final temperatures of each cycle are T_{f1}=40°C; T_{f2}=50°C; T_{f3}=70°C; T_{f4}=100 ° C and T_{f5} =100 °C.

Table 6. Glass transition temperature at the onset, midpoint and end obtained on successive heating of the sample FNB@MSNs_APTES during the gradual drying treatment and respective heat capacity.

	$T_{g\text{-}on}$ (ºC)	$T_{g\text{-}mid}$ (ºC)	$T_{g\text{-}end}$ (ºC)	ΔC_p (J/gºC)
After T = 40 ºC	-22.31	-17.69	-10.69	0.06662
After T = 50 ºC	-21.77	-16.33	-13.59	0.04053
After T = 70 ºC	-19.47	-7.24	-3.22	0.03817

Finally, the guest physical state was also accessed in the FNB@MSNs_TMPS composite. Thermal gradual drying was performed at 10°C/min and following the same heating/cooling cycles (inset of Figure 26). The heating thermograms show the gradual removal of water content and a clear step associated to the glass-liquid state transformation.

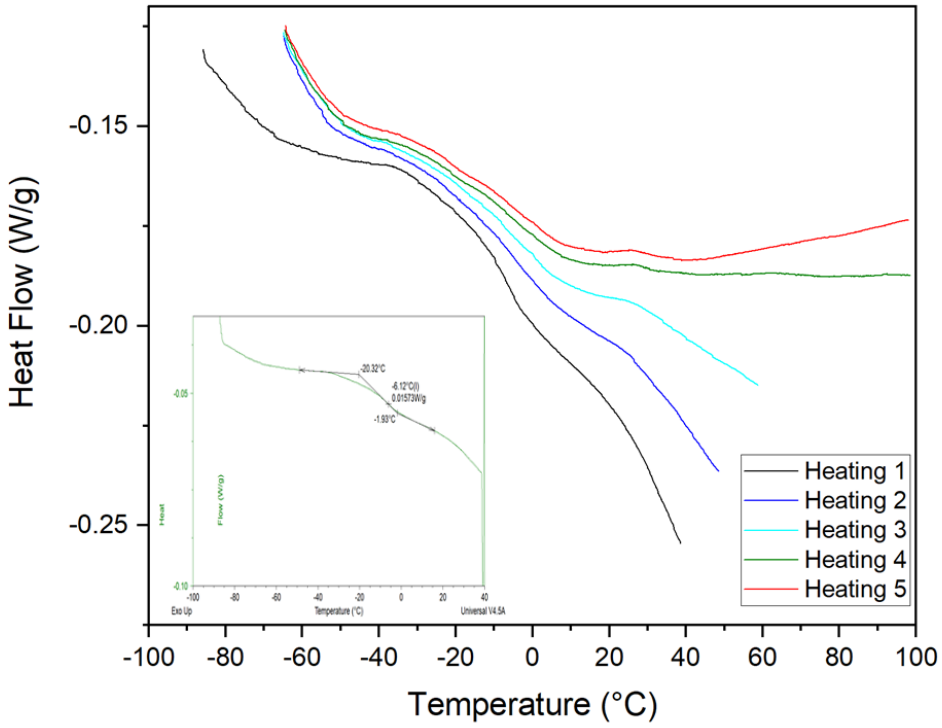

Figure 29. Heating thermograms at 10 ºC/min of the sample FNB@MSNs_TMPS obtained with gradual heating. Inset shows the enlarged glass transition region on heating 1. The final temperatures of each cycle are T_{f1} = 40°C; T_{f2} = 50°C; T_{f3} = 70°C; T_{f4} = 100°C; T_{f5} = 100°C.

On the other hand, no signal of melting of FNB is detected which indicates that FNB is totally in the amorphous state. It seems important to note that in this sample, the relation of masses between MSNs and FNB is different to the other two samples, with more quantity of loaded FNB. Then, if some fraction of FNB would not be interacting with the silica (directly or with the functional groups) it would be more

expectable the existence of a crystalline fraction. The temperatures of the onset, $T_{g,ons}$, midpoint, $T_{g,mid}$, and endset, $T_{g,end}$, of the detected glass transitions are presented in Table 7.

Table 7. Glass transition temperature at the onset, midpoint and end obtained on successive heating of the sample FNB@MSNs_TMPS during the gradual drying treatment and respective heat capacity.

	$T_{g\text{-}ons}$ (ºC)	$T_{g\text{-}mid}$ (ºC)	$T_{g\text{-}end}$ (ºC)	ΔC_p (J/gºC)
After T = 40 ºC	-20.32	-6.12	-1.93	0.01573
After T = 50 ºC	-20.14	-4.22	3.55	0.01345
After T = 70 ºC	-17.98	-6.93	3.52	0.001147

As we said above, the interval of glass transition temperature was defined by the onset of T_g and $T_{g\ onset}$ were analyzed only for cycles until temperature of 70 °C because at higher temperature was more difficult to detect the change in the heat flow line. A more direct comparison of only $T_{g\text{-}onset}$ values between the three samples is reported in Table 8.

Table 8. $T_{g\text{-}\ onset}$ values of FNB in MSNs, MSNs_APTES and MSNs_TMPS under gradual heating until 70°C, [b] up to 100°C

Sample	$T_{g\text{-}ons}$ (°C) Heating 1	$T_{g\text{-}ons}$ (°C) Heating 2	$T_{g\text{-}ons}$ (°C) Heating 3
FNB@MSNs	-23.64	-22.68	-21.32[b]
FNB@MSNs_APTES	-22.31	-21.77	-19.47
FNB@MSNs_TMPS	-20.32	-20.14	-17.98

Remembering, all the composites had revealed to retain an amount of adsorbed water on the silica that accentuate T_g reduction by the plasticization effect. Based on this, although MSNs_APTES had showed to retain a more amount of water compared to the bare MSNs, the modifying agent creates some drug-particle interactions that slightly leads to an increase in T_g especially at 70°C when the water is progressively removed. From the thermogram in figure 29 and the corresponding T_g values in Table 7, a more accentuated shift toward higher temperature of the glass transition in the third heating is observed in nanoparticles modified with TMPS. It could indicate that interactions between TMPS and FNB are stronger than interactions found between APTES and FNB. However, this value does not exceed the value of native FNB (T_g=-17.71 [38]) even at 70°C suggesting that the plasticization effect persist. Also, this increase is not very significant probably due to the low functionalization of the silica nanoparticles with this agent as it is presented in the ^{1}H NMR studies (0.60 molecules/nm^2). On the other hand, amine functionalization was successfully achieved (1.93 molecule /nm^2) but it did not bring to significant increase in $T_{g\text{-}onset}$ values suggesting that the interaction with the drug is not strong enough and nanoconfinement and plastification effects prevail.

Though, given that the matrixes have the same pore and diameter size, the differences found in the guest glass transition arise mainly from the different modifying agents used to functionalize mesoporous silica nanoparticles.

Figure 30 shows a comparison of the heat flow change during the first heating for fenofibrate inside bare and functionalized silicas matrixes. However, it is important to note that the $T_{g\text{-}ons}$ is still below 25°C in all the composites meaning that at room temperature fenofibrate in its amorphous state is inside the pores in the supercooled liquid state.

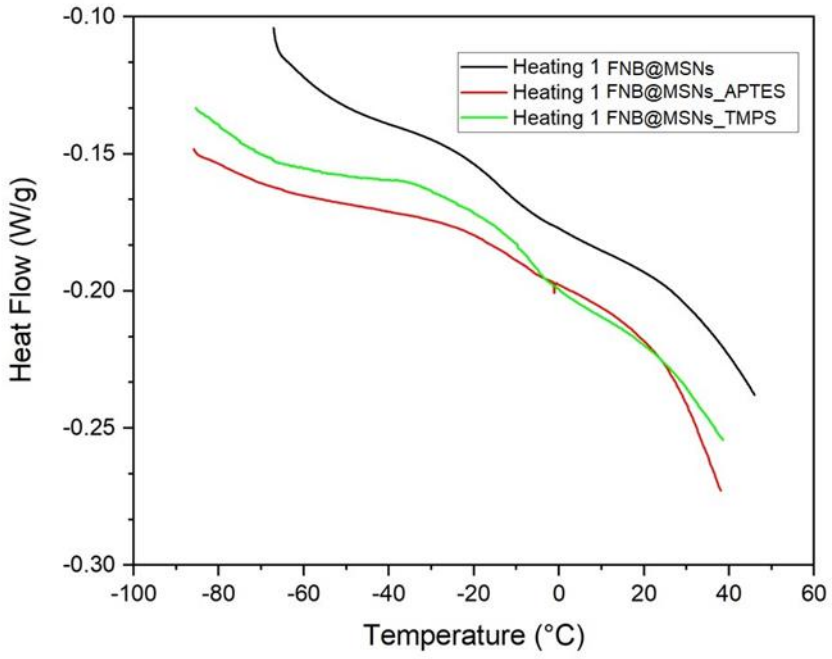

Figure 30. Heat flow change of FNB. Heating 1 up to 50°C for FNB@MSNs and heating 1 up 40°C for FNB@MSNs_APTES and FNB@MSNs_TMPS.

3.4.2 DRS RESULTS

The characterization of the glass transition behavior is rather important in order to predict stability. However, storage below T_g is not a guarantee of stability since the residual molecular mobility, which is still preserved in the glassy state can induce devitrification. Thus, dielectric relaxation spectroscopy (DRS) was used since it is an excellent technique to probe the molecular mobility of the guest and to access the time scales of the relaxation processes. DSC results had shown a greater amount of water entrapped in the MSNs_APTES compare to the bare MSNs. This is also confirmed by DRS studies. The dielectric module values obtained at 10^5 Hz for bare and functionalized MSNs of two different series of isothermal acquisition data up to 150 ºC are compared In Figure 31 (note that the first series acts as a drying treatment). Regarding bare MSNs two maximum below 50°C are detected in series 1 (light blue) while none is detected in series 2 (orange) indicating that they correspond to a dipolar motion of water. On the other hand, MSNs_APTES still present a relaxation peak even in the second series (red) confirming that some traces of water molecules are still adsorbed on the silica (heating after drying).

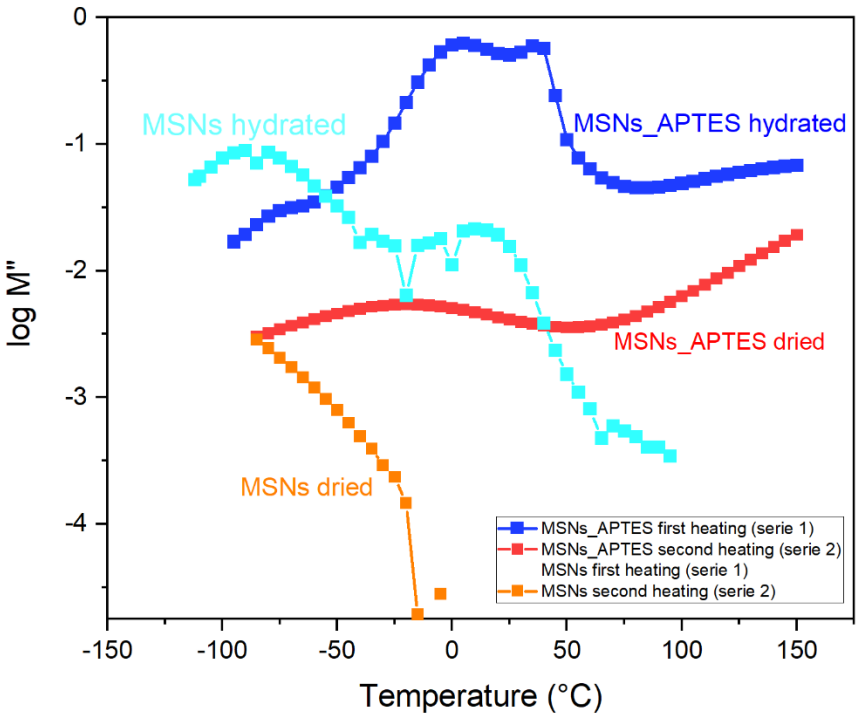

Figure 31. M" *vs.* T plot at 10^5 Hz of MSNs (series 1 and 2) and MSNs_APTES (series 1 and 2) representing the different amount of water that remains adsorbed on the silicas after the first heating up to 150°C.

To better visualize how the water content is removed, the real part of the permittivity, ε´, has been represented versus temperature at f = 0.1 Hz (Figure 32) for data on the first and second series. Here differences between samples can be better understood. In both samples, during the first heating, ε´ increases up to close 0°C. Then, after a bimodal shape more clearly defined in MSNs_APTES, ε´ decreases in different ways. In bare MSNs (Figure 32 (a)) the final value attained at 150°C is lower than that at -100°C due to the completely loss of water, as it is confirmed in the second heating, while in MSNs_APTES (Figure 32 (b)), ε´ attains a value higher than that one at lower temperature suggesting that the water is not totally removed from the sample and it persists into the silica even at high temperature up to 150°C as it is represented also in series 2 .

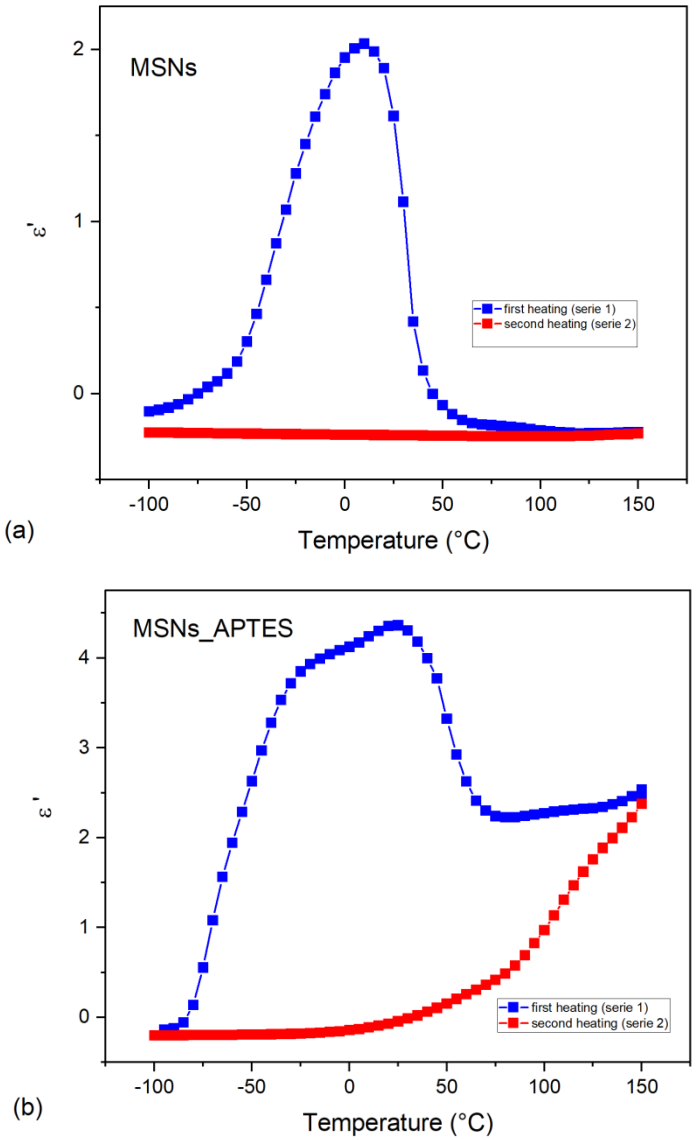

Figure 32. ε´ *vs.* T plot at 0.1 Hz of: (a) MSNs and (b) MSNs_APTES; blue and red data correspond to series 1 (hydrated) and series 2 (dried) respectively.

Figure 33 and Figure 34, show the dielectric modulus of fenofibrate in MSNs and MSNs_APTES at the frequency of 10^5 Hz. Data of native amorphous FNB has been included for comparison. Isochronal line of series 1 in Figure 33 (blue line) shows three relaxation peaks: the first two at lower temperatures are principally related to water and the third one is related to the fenofibrate in silica. By comparing with the α process in the native fenofibrate (that it is associated to the dynamic glass transition), this third process is shifted to higher temperatures and apparently independent of water content (series 1 and 2 seems to coincide in this figure). The profile observed in M´´ is similar to that observed in ε'' (data not shown) which means that all processes above referred have a dipolar origin and are not related to charge translational motion. It is important to be noticed that in the spectra of native fenofibrate around 50°C a sharp decrease appears due to the recrystallization followed by a sharp increase some degrees above that corresponds to the melting of the crystal formed. The motion of dipoles in the glassy/supercooled liquid was hindered by the recrystallization leading to a reduction in M´´ (and ε''). On the other hand, with melting, dipole of the molecules achieves again mobility. The observed increase above melting (around 80 °C) in Figure 33 and in Figure 34 occurs at temperatures higher than the alpha process (at this frequency) where the sample shows conductivity. Thus, DRS spectroscopy again leads to affirm that amorphous fenofibrate is not stable and it has tendency to recrystallize while no signal of melting is observed when is loaded in mesoporous silica nanoparticles, in accordance with thermograms obtained by DSC.

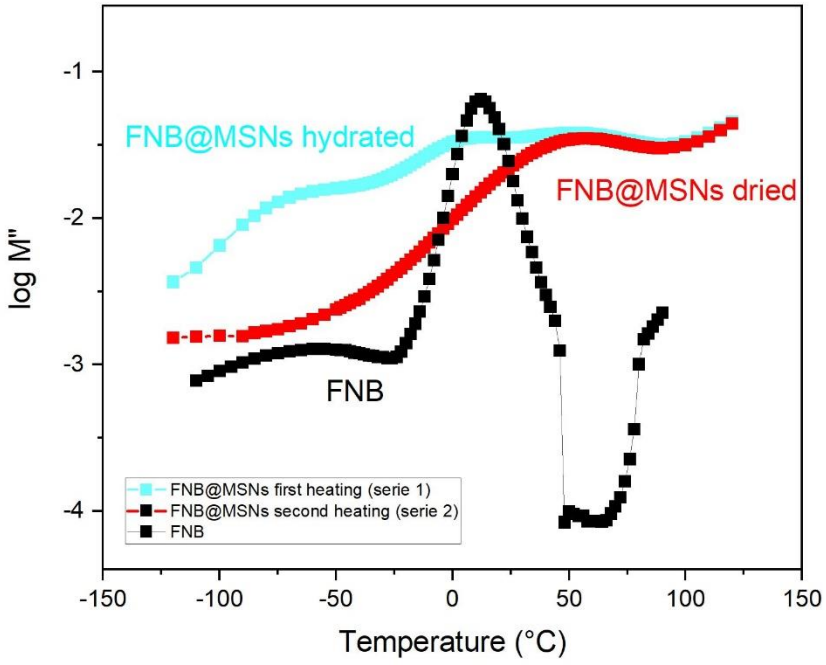

Figure 33. Isochronal representation of M´´ *vs.* T at 10^5 Hz for native FNB (black squares), FNB@MSNs series 1 (hydrated) in light blue, and series 2 (dried) in red.

Concerning fenofibrate incorporated in functionalized silica with APTES, the isothermal spectra collected show that still some amount of water is retained in the second series indicated by the approximation of the two lines at lower temperature (a relaxation process of water is even observed). This higher adsorbed amount of water in silica modified with APTES could be probably due to the hydrogen-bond formation between water molecules with the amino groups of the modifying agent. Also, the maximum positions of M´´ of FNB in MSNs_APTES is closer, at this frequency, to the maximum position of native FNB than of FNB in bare MSNs. This similarity of temperatures in the two relaxation processes (native and incorporated FNB) has to be confirmed with fitting procedures.

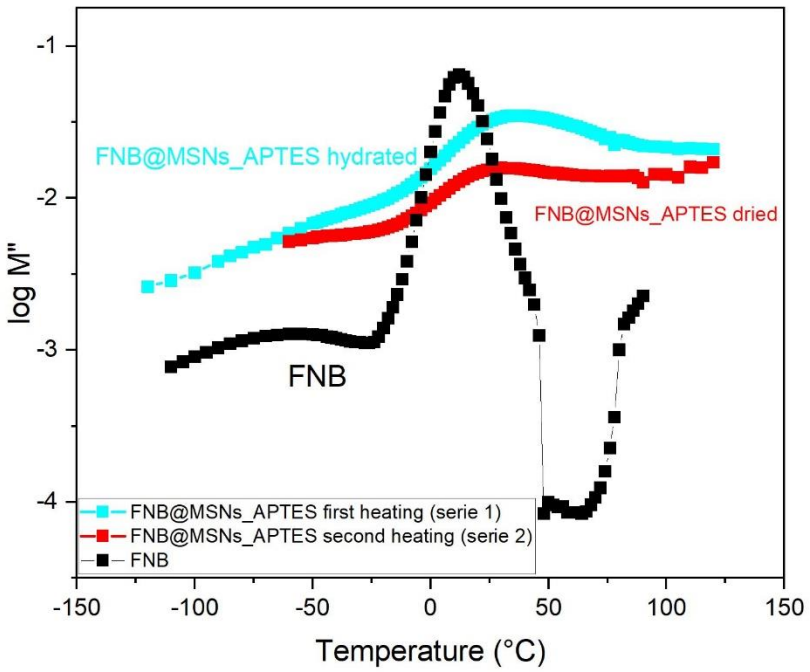

Figure 34. Isochronal representation of M´´ *vs.* T at 10^5 Hz for native FNB (black squares), FNB@MSNs_APTES series 1 (hydrated) in light blue, and series 2 (dried) in red.

Figure 35 shows data of MSNs_APTES at frequencies higher than 10^5 Hz, where a small discontinuity at 78.2°C (dash dot red line) appears nearly independently of frequency. The presence of this peak could be attributed to the melting of the small crystalline fraction of FNB already observed in the DSC thermogram. It is important to underline that the presence of this peak related to the melting temperature of fenofibrate is only present in the first scan of the sample up to 150°C. The second series did not reveal it because once the crystals melt, fenofibrate did not crystallize again. Thus, all fenofibrate molecules upon the second heating will be stable in the disordered amorphous state inside silica matrix.

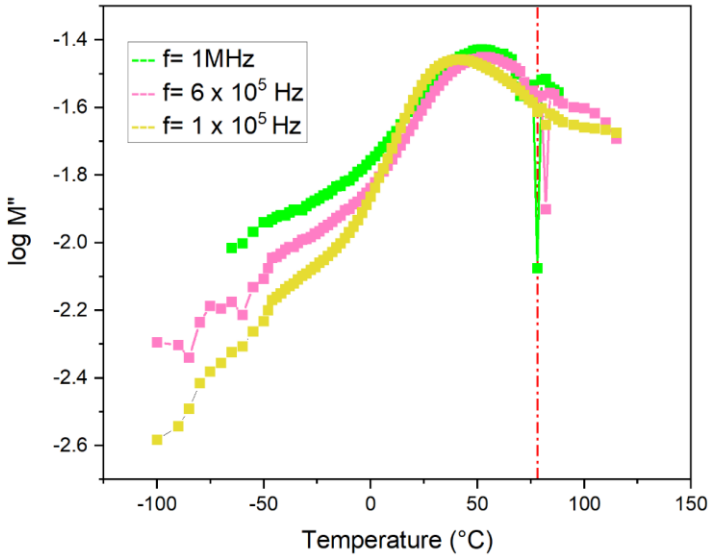

Figure 35. Isochronal representation of M´´ *vs.* T at 1MHz, 6 x10^5 and 10^5 Hz of FNB@MSNs_APTES.

In the following, the mobility of the amorphous fenofibrate into the silicas is analyzed. Figure 36 shows the isochronal plots of M´´ for all the frequencies available from 0.1 Hz to 10^6 Hz and from temperatures between -120 and 120°C.

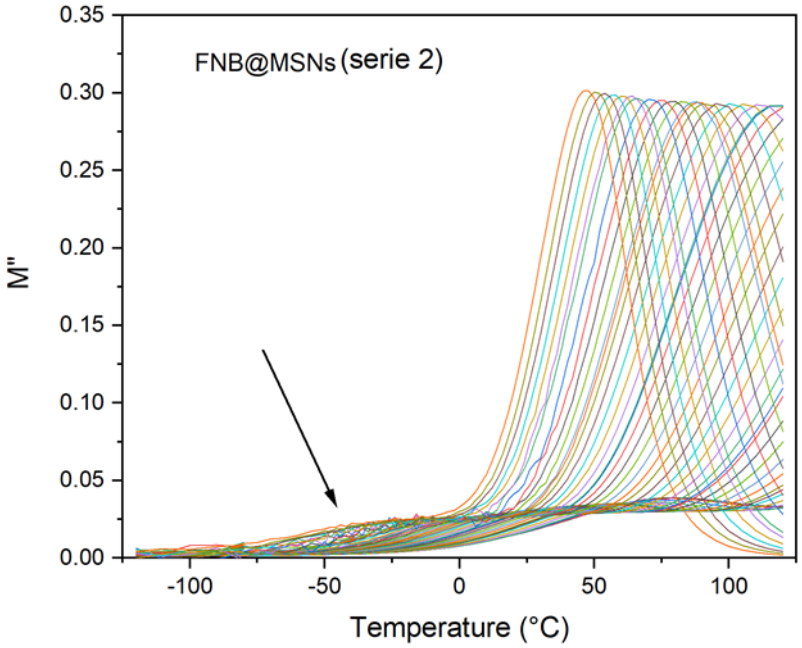

Figure 36. Isochronal representation of M´´ collected in the isothermal mode from -120 to 120°C covering the frequency range from 0.1 Hz up to 1 MHz for the sample FNB@MSNs in the second series. The arrow indicates the relaxation process of constrained FNB.

To better investigate the dynamic behavior of fenofibrate in bare and functionalized silica nanoparticles, peaks observed in the isochronal representation of M´´ have been individually analyzed. It must be underlying that only isothermal spectra acquired in the second isothermal heating series were analyzed given that during the first isothermal scans, sample is changing due to the progressive removal of water (series 1 acts as a drying procedure). However, data from the first series were helpful to confirm that fenofibrate was mostly in amorphous state when it is included in silica matrixes. The deconvolution of each isochronal data of M´´ was done by the superposition of one or two gaussians peak functions. Figure 37 represents M´´ *vs.* T at the frequency of 95.24 Hz where the solid lines correspond to individual and overall fitting of raw data (open symbols). For this frequency, data for lower temperatures were not considered since the focus of this analysis was principally on the supercooled region ($T \geq T_g$) and not on the glassy state (below T_g).

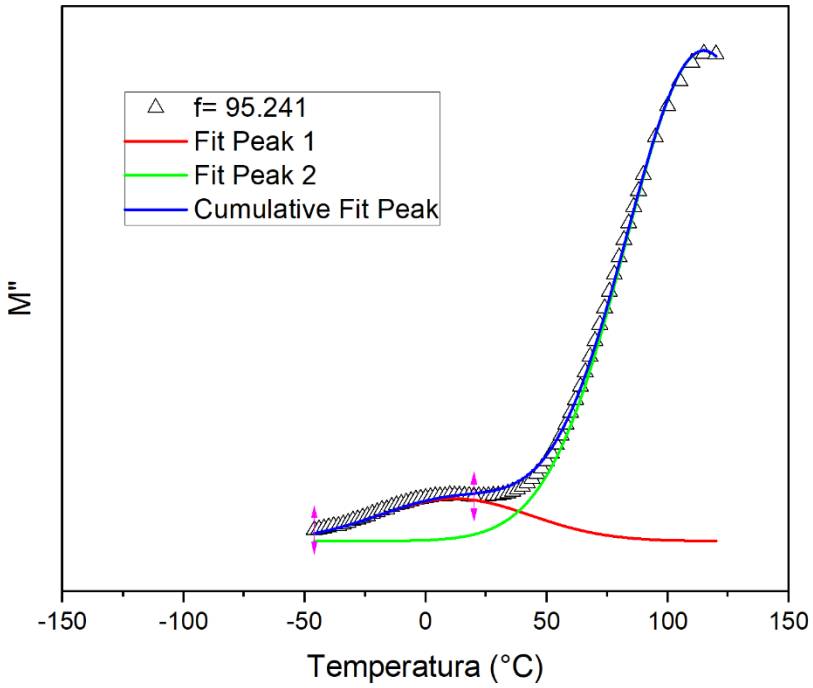

Figure 37. Dielectric loss of fenofibrate versus temperature at frequency of f = 95.241 Hz confined to the bare MSNs; the solid lines (red and green) are the two gaussian summed to simulate the isochronal plot of FNB@MSNs above -50°C. The overall global fit is included (blue line).

From this analysis, for each frequency it has been estimated the temperature position of each peak observed, i.e. pairs as (f, T_{max}). The relaxation time characteristic of each process depends on the mobility of the molecules (dipoles) that constitute a material. It corresponds to the time during which the polarization created in the material by the external electric field decays, after the field is removed, by a factor 1/*e*, where *e* is the Neper number.

The relaxation time was calculated as:

$$\tau_{max} = 1/2\pi f \qquad \text{(Equation 2)}$$

and then its temperature dependence has been represented in the relaxation map, -log (τ_{max} *vs.* 1000/T), that is plotted in Figure 38. In this plot has been also included the relaxation times estimated for bulk fenofibrate for comparison (in this case, the temperature of maxima has been taken directly from the isochronal representation, without fitting).

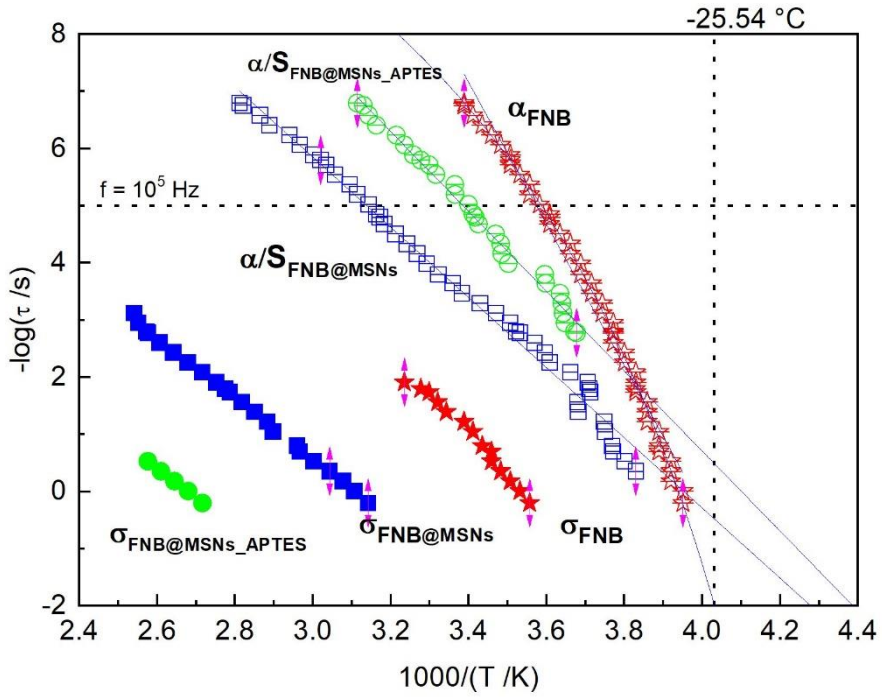

Figure 38. Temperature dependence of the relaxation times of each process observed in: red symbols for bulk amorphous FNB (in this sample, the temperature position was taken directly from the M´´ *vs*. T representation, i.e., without mathematical deconvolution of peaks); blue symbols for FNB@ MSNs, and green samples for FNB@MSNs_APTES. Solid lines correspond to the respective Arrhenius and VFTH curve fits. Dot vertical line show the T_g of amorphous FNB taken dielectrically and the dot horizontal one indicate a fix frequency for better comparison.

In bulk amorphous FNB, in the temperature analyzed, two processes were detected, one of them related to the glass transition designated as alpha process [37] and the other one, at highest temperatures, related to conductivity (translational motion of charges).

Concerning the α, the relaxation time follows a curvature in -logτ *vs.* 1000/T that can be described by the empirical VFTH (Vogel Fulcher Tamman Hess [59]) equation:

$$\tau(T) = \tau_\infty e^{\frac{B}{T-T_0}} \qquad \text{(Equation 3)}$$

with parameters B = 1722.08 K, T_0 = 204.8 K and $\tau\infty = 10^{-15.01}$ s.

The glass transition temperature was estimated from dielectric data by extrapolating the fitted curve at τ = 100 s. This value comes from the Maxwell relationship between viscosity (η) and the shear modulus G given by η = Gτ assuming for a solid material a viscosity of ~10^{12} Pa s and G ~ 10^{10} Pa. [60]

With VFTH parameters obtained for bulk FNB, the T_g estimated at τ = 100 s is -25.5°C. This value is lower than the T_g = -17.7ºC reported in reference [38]. Such difference can be easily explained due to: (i) T_g is taken from two different techniques and (ii) the analysis of dielectric data in M´´ provides lower values than that provided by the analysis of ε''. On the other hand, relaxation times obtained for FNB@MSNs and FNB@MSNs_APTES samples show a linear temperature behavior in the relaxation map that can be described according to:

$$\tau(T) = \tau\infty exp(Ea/RT) \quad \text{Equation 4}$$

For FNB inside bare MSNs and MSNs_APTES, the Arrhenius equation (Equation 4) ,was used to estimate the corresponding T_g .The values of the activation energies, T_g and the values of the pre-exponential factors, both of the processes in FNB constrained in silica and the alpha process in bulk FNB, are included in Table 9.

Table 9. Glass transition temperatures, activation energy and$\tau\infty$ values for native drug, FNB@MSNs and FNB@MSNs_APTES determined from dielectric data.

Sample	E_a (kJ/mol)	$\tau\infty$ (s)	T_g (°C) (τ = 100 s)
FNB@MSNs	118	6.31×10^{-25}	-39.18
FNB@MSNs_APTES	135	2.13×10^{-29}	-45.24
Bulk FNB	463	9.7×10^{-16}	-25.54

As it can be noted, the T_g of FNB loaded inside silicas are significantly lower than that of bulk FNB which could suggest a strong confinement effect. However, given that the deviation observed by DSC is less accentuated, even considering the plasticization effect of water for inefficiency of the drying treatment (series 1), it seems less probable to be a true confinement effect. Additionally, it must be also considered that relaxation times of this process have been obtained well above T_g, and it is possible that approaching to T_g, a curvature in the relaxation times occurs.

In order to understand the origin of this process detected in FNB loaded in silicas it is interesting to look at the activation energy. In loaded FNB, the E_a estimated from the Arrhenius equation (Equation 4) was 118 and 138 kJ/mol for FNB@MSNs and FNB@MSNs_APTES respectively.

For bulk FNB, the activation energy must be estimated as:

$$Ea = \mathrm{R}\frac{\partial ln\tau}{\partial\left(\frac{1}{T}\right)} = \frac{RB}{\left(1-\frac{T}{T_0}\right)^2} \qquad \text{(Equation 5)}$$

that it allows to calculate the activation energy at each temperature. By replacing the glass transition temperature of bulk fenofibrate (T_g = -25.24ºC), the E_a associate to this mechanism gives a value of 463 kJ/mol not far from the data reported in reference [38] obtained with other technique.

As it is noted, the activation energy of FNB in nano matrixes is significant lower to that in the native form. It could be rationalized that the mechanism involved is more localized. It has been reported [37] that FNB presents a secondary process, γ, even active in the glassy state. However, the activation energy indicated for this localized motion was 32.67 kJ/mol, significantly lower than that found in FNB incorporated in silica nanoparticles, which leads to put apart this interpretation.

A decrease in the activation energy could be due to a change in the temperature dependence of the alpha relaxation, from a VFTH behavior above T_g, to an Arrhenius (linear) behavior, below T_g. [61] However, this is not the case observed in FNB@MSNs and FNB@MSNs_APTES in which the linear trend is found well above the T_g.

Another possible explanation for this process can be related to FNB molecules adsorbed to silica surface, both outside the nanoparticles and inside the pores. This type of motions has been found in similar nanocomposites. [61,62] and arise from a higher hindrance imposed by only the silica pores walls. This mechanism usually is originated at temperatures above T_g and a linear or a curvature temperature behavior in the relaxation map appears. Concerning the activation energy, it is lower than that characteristic of the α process. Another important subject that can reinforce this hypothesis refers to change in the heat capacity observed by DSC. It has been reported [63] that the ΔC_p associated to the glass transition is no more observed if the percentage in mass is lower than 20% and a thin layer of molecules is formed. In FNB, in fact, the ΔC_p at T_g is visible in the hydrated samples, and it progressively becomes undetectable as water is removed, which would be compatible with a more approaching of FNB molecules to surface and the formation of a very thin layer.

Anyway, more work should be done to clarify the origin of this relaxation mechanism.

Although experiments on FNB@MSNs_TMPS were not performed for lack of time, the results obtained for FNB@MSNs_APTES and FNB in bare MSNs (FNB@MSNs) are indicative of the effect of silica functionalization on the behavior of FNB. As temperature increase above the T_g, the relaxation time of the process, of FNB constrained into silicas, is located at lower frequencies than that observed in bulk FNB, meaning that the molecules involve relax with a slower relaxation rate than that in bulk amorphous material. In other words, at the same frequency, FNB molecules need higher temperature to reach the same molecular mobility of the bulk fenofibrate.

3.5 RELEASE STUDY

The solution media for drug release was composed by phosphate buffer at pH 8 and ethanol in the w/w proportion of 90:10. Ethanol was chosen due to the higher solubility of FNB in this medium than aqueous medium. [64] Base Line was done with a quartz cuvette with 3 mL of the PBS: ethanol solution. Drug release was monitored during 8 hours by UV-Vis following the procedure developed in the laboratory [65]. A dialysis tube with a cellulose membrane divides the top chamber from the bottom chamber of a quartz cuvette (Figure 9). The sample (MSNs and FNB) in 200 µl of PBS/EtOH (10%) was added to the top chamber. The bottom chamber was filled with 3.3 mL of the solution media (PBS/EtOH mix) and kept under continuous stirring at 400 r.p.m. Successive UV-VIS spectra (200 to 700 nm) was collected at an acquisition rate of 400 nm/min. During the first 4 hours, spectra was taken every 60 seconds and then, every 600 seconds until complete 8 hours. To analyse the release profile, absorbance at λ = 289 nm was represented as a function of time (Figure 39). For both samples (APTES and TMPS functionalized MSNs), a gradual increase of the absorbance due to fenofibrate release is observed and there is no initial faster diffusion of FNB molecules from both composites indicating that mostly all the FNB molecules should be located deeper inside the silica pores.

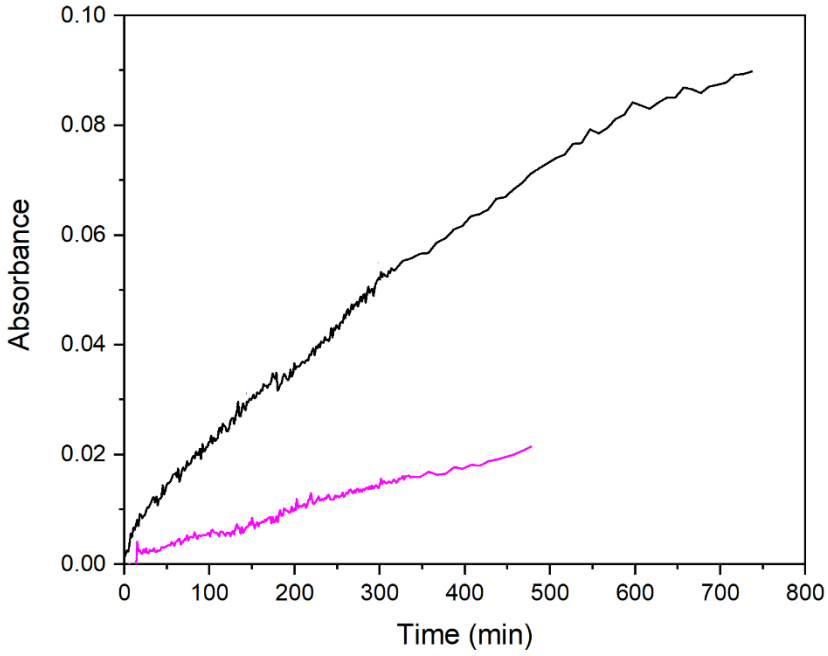

Figure 39. Release profile of FNB@MSNs_APTES (black line) and FNB@MSNs_TMPS (pink line) obtained at λ = 289 nm.

Considering that very similar masses of both samples were put in the cuvette it can be concluded that the release from FNB@MSNs_APTES is faster than from FNB@MSNs_TMPS. To estimate the concentration of FNB a calibration curve was measured for FNB in PBS/EtOH (10%) yielding a FNB molar absorption coefficient of $\varepsilon = (15.2 \pm 0.5) \times 10^{-3}$ cm^{-1} M^{-1} (Figure 40).

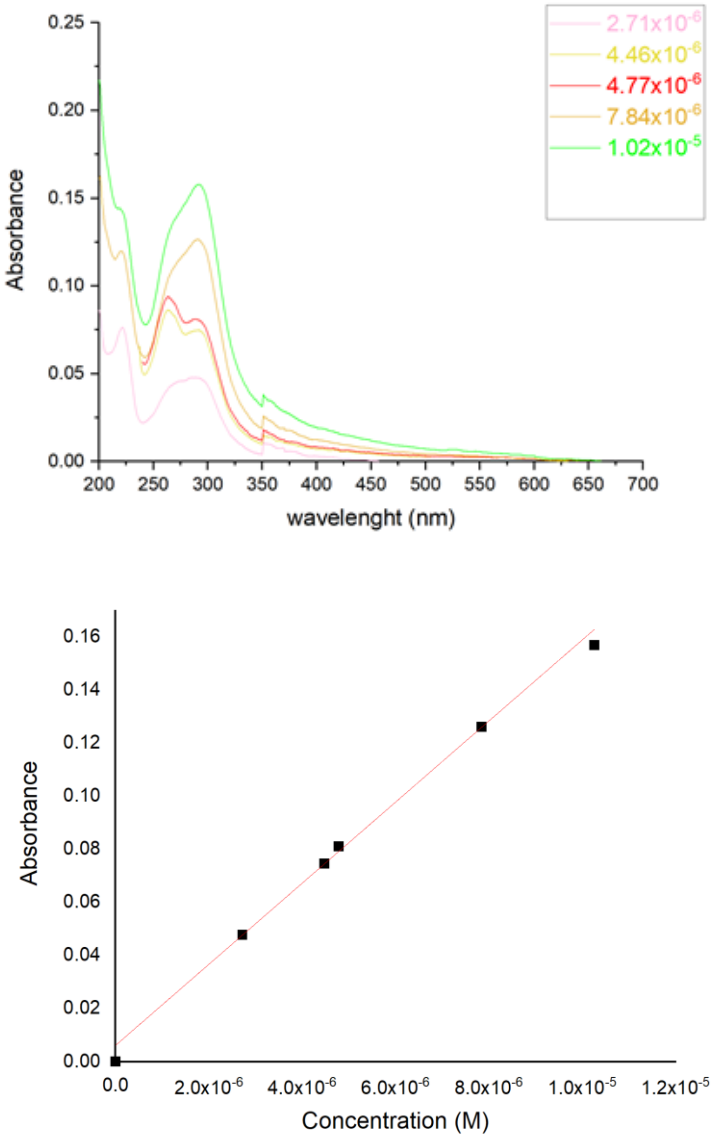

Figure 40. Absorption spectra of FNB solutions in PBS/EtOH at λ = 289 nm, inset shows the respective concentrations in [mol/L] (top) and corresponding calibration curve (bottom). $Abs = (15.2 \pm 0.5)x10^3\ C + (0.005 \pm 0.003)$ with $r^2 = 0.996$.

With this curve, and since the volume in the bottom compartment of the dialysis is constant, it was possible to obtain the evolution of the number of moles released during the experiment. The fenofibrate concentration can be estimated allowing to find its dependence with time during release in the cuvette. In Table 10 are summarized the number of moles release from each sample at the end of 8 hours. From the concentration vs. time plot it was possible to estimate the amount of fenofibrate released.

Table 10. FNB released after 8 hours

Sample	m_{MSNs}(g)	m_{FNB} (g)[a]	n_{FNB} (mol)[b]	n_{MSNs} (mmol/g) [c]	n_{rel} (mmol/g) [d]	$n_{Released}$ (%) [e] (after 8h)
FNB@MSNs_APTES	1.73×10^{-3}	0.39×10^{-3}	1.09×10^{-6}	0.332	9×10^{-3}	2.7
FNB@MSNs_TMPS	1.63×10^{-3}	0.54×10^{-3}	1.50×10^{-6}	0.729	3×10^{-3}	0.4

[a] grams of FNB in MSNs, [b] number of moles of FNB in MSNs, [c] number of FNB moles in the MSNs per gram of nanoparticles, [d] number of moles of FNB released after 8 hours per gram of MSNs; [e] percentage of moles released after 8 hours (relative to loaded FNB).

Data reported in Table 10 indicate a slower release of FNB from MSNs_TMPS. Since the experiments were performed with almost the same concentration of nanoparticles in the upper compartment, we conclude that FNB diffuses more slowly from the pores of the MSNs_TMPS than MSNs_APTES. This is probably due to the stronger interactions of FNB with the trimethoxy(phenyl)silane groups at the pore surface, and also to the bulkier structure of this group compared to APTES. Also, despite the higher amount of FNB incorporated in the MSNs_TMPS (up to 33.3 wt%) compared to MSNs_APTES (22.8 wt%), the concentration of FNB in the cuvette at the end of 8 hours corresponds to less than 0.5% for MSNs_TMPS, and to 2.7 % for MSNs_APTES.

Therefore, MSNs_TMPS presents higher FNB loading capacity and slower release kinetics due to stronger interaction between FNB and TMPS. On the other hand, MSNs_APTES shows faster FNB release kinetics, suggesting weaker FNB/APTES interactions.

It was not possible to follow the release kinetic from bare MSNs because there was almost no fenofibrate released during the time of the analysis (8h). This could be due to the dialysis membrane preventing the diffusion of FNB; however, this is not the case since FNB is released from the functionalized MSNs. The explanation is probably a strong interaction between FNB and the silica matrix, with the drug-pore adsorption energy balancing the osmotic pressure for FNB to be released. [28]

4. CONCLUSIONS

Mesoporous silica nanoparticles (MSNs) with (49 ± 6.6) nm of external diameter and regular pores of 3 nm have been prepared. The external and internal surface of these MSNs was modified with organic alkoxysilanes containing functional groups with different polarity; hydrophilic 3-(Aminopropyl)triethoxysilane (APTES) and hydrophobic trimethoxy(phenyl)silane (TMPS).

The modification was confirmed by ^{1}H NMR. The surface density of functionalization calculated for APTES and TMPS are 1.93 and 0.6 molecules/nm^2, respectively. Subsequently, fenofibrate (FNB), a low soluble drug was loaded in the three different silicas (bare MSNs, MSNs_APTES and MSNs_TMPS) to achieve its amorphization and to control its release.

FTIR spectra show that fenofibrate is clearly absorbed in the matrix and it interacts with the silica surface. Uv-vis spectroscopy was used to evaluate the fraction of FNB directly interacting with the silica surface. As expected, this amount depends on functionalization, resulting from the different hydrophobicity and hydrophilicity of the functional groups. Especially, the similar hydrophobicity of the TMPS group and the drug give rise to stronger interactions. This was confirmed looking at the mmol/g of FNB in each samples after be washed (corresponding to 0.729 mmol/g of FNB per gram of MSNs_TMPS and to 0.245 mmol/g of FNB in bare MSNs). Thus, the loading capacity of MSNs specific to FNB can be improved via precise functionalization.

A set of techniques, including calorimetry (DSC) and dielectric relaxation spectroscopy (DRS) were used to obtain detailed information on the physical state of the loaded FNB.

DSC shows that full FNB amorphization was successfully achieved (except for a very low fraction of FNB loaded in MSNs_APTES) and in DSC the T_g was detected in the three composites at lower temperatures than the T_g of bulk FNB. Additionally, the temperature range in which the material undergoes a second order phase transition (i.e., liquid to glass or vice versa), is larger with respect to the one in native fenofibrate because of the interaction with the silica. Moreover, the DSC analysis shows a higher amount of water adsorbed in MSNs modified with APTES probably due to the presence of hydrogen bonds between water molecules with the amino groups of the modifying agent.

The molecular mobility of the loaded drug was investigated by dielectric relaxation spectroscopy (DRS). By analyzing the dielectric modulus of fenofibrate in bare MSNs and MSNs_APTES , no signal of melting is observed when FNB is loaded in mesoporous silica nanoparticles (in accordance with thermograms obtained by DSC), confirming that FNB is stabilized in its amorphous disordered state. Moreover, in FNB loaded in bare MSNs and MSNs_APTES samples, a dipolar mechanism is clearly observed, and it is shifted to higher temperatures/lower frequencies relatively to the α process (associated to the glass transition) of bulk FNB. The glass transition temperatures estimated from dielectric data are significantly lower than the T_g determined by differential scanning calorimetry (DSC). This fact, together with the Arrhenius temperature dependence and a relatively low activation energy, suggests a surface process and not a true α relaxation (nevertheless more work must be done to fully confirm this hypothesis).

Additionally, this relaxation mode is faster when FNB is loaded in MSNs_APTES than in bare MSNs, indicating that the presence of APTES induces weaker interactions with FNB. The residual water in this sample (not removed by drying) may also contribute to this enhanced mobility. Although experiments on FNB@MSNs_TMPS were not performed for lack of time, the results obtained for FNB@MSNs_APTES and FNB in bare MSNs (FNB@MSNs) are indicative of the effect of silica functionalization on the behavior of FNB.

The release of FNB from the MSNs was followed by UV-Vis spectroscopy, showing that MSNs_APTES provide faster FNB release kinetics than MSNs_TMPS in a period of 8 h. The fact that the amount of FNB released form functionalized silicas is very low in the period of 8h, indicates that both systems are able to control the release process for a long period of time.

In conclusion, by tuning the pore functionality of MSNs, it is possible to stabilize the amorphous state of the crystallizable drug fenofibrate, and also to modulate the drug release kinetics, to fit the desired applications.

5. FUTURE STUDIES

In further studies, it could be interesting to perform nitrogen adsorption to obtain the surface area by BET method (Braunauer-Emmet-Teller method) and pore diameter and volume by the BJH method (Barret-Joyer-Halenda method) of functionalized and bare MSNs in order to verify if there are significant changes between nanoparticles functionalized and not. Also, characterization of functionalized MSNs_APTES and MSNs_TMPS by TEM could be interesting to evaluate if the structure of these nanoparticles was well preserved even after functionalization processes. It should be of great interest also to explore the molecular mobility of FNB inside MSNs_TMPS and thus maybe clarify the origin of the relaxation process of FNB loaded in silicas. Finally, release of FNB for longer times should be performed.

6.BIBLIOGRAPHY

[1] S. Baghel, H. Cathcart, N. J. O'Reilly, Solid Dispersions: A Review of Amorphization, Crystallization, Stabilization, Solid-State Characterization, and Aqueous Solubilization of Biopharmaceutical Classification System Class II Drugs, *Journal of Pharmaceutical Sciences* ,105 (9), 2527-2544,**2016**

[2] Savjani K.T, Gajjar A. K., Savjani J. K., Drug Solubility: Importance and Enhancement Techniques, *ISRN Pharmaceutics Volume*, Article ID 195727,**2012**

[3] Amidon G. L., Lennernäs H., Shah V. P., Crison J. R., A theoretical basis for a biopharmaceutic drug classification: The correlation of in vitro drug product dissolution and in vivo bioavailability, *Pharmaceutical Research*, 12, 413–420, **1995**

[4] Sachan N.K., Pushar S., Mishra A., Biopharmaceutical classification system: a strategic tool for oral drug delivery technology, *Asian journal of pharmaceutics*,3(2) **2009**

[5] Serajuddin A.T.M., Salt formation to improve drug solubility, *Advanced Drug Delivery Reviews.*,59, 603-619,**2007**

[6] Bernstein J., Polymorphism in molecular crystals, *IUCr monographs on crystallography* ,volume 14,**2002**

[7] Censi R., Di Martino P., Polymorph Impact on the Bioavailability and Stability of Poorly Soluble Drugs, *Molecules* ,*20*, 18759-18776,**2015**

[8] Hancock B., Parks M., What is the true stability advantage for amorphous pharmaceuticals?, *Pharmaceutical research 17(4):397-404*,**2000**

[9] Ghule P., Gilhotra R., Jithan A., Bairagi S., Aher A., Amorphous solid dispersion: a promising technique for improving oral bioavailability of poorly water-soluble drugs, *S. Afr Pharm J,* 85(1): 50-56, **2018.**

[10] Hong S. , Shen S., Tan D. C. T., Kiong W., LiU X., Chia L. S. O., Irwan A. W., Tan R., Nowak S.A., Marsh K., Gokhale R., High drug load, stable, manufacturable and bioavailable fenofibrate formulations in mesoporous silica: a comparison of spray drying versus solvent impregnation methods ,*Drug delivery, 23(1),316-327,**2016***

[11] Kresge C. T., Leonowicz M. E.,Roth W. J, Vartuli J. C., Beck J. S. ,Ordered mesoporous molecular sieves synthesized by a liquid-crystal template mechanism, *Nature*, 359, 710-712,**1992**

[12] Valet-Regi M., Ramila A., Del Real R. P., Pérez-Pariente J., A New Property of MCM-41: Drug Delivery System, *Chem. Mater*, 13, 308-311,**2001**

[13] Shen S-C., Ng W. K., Chia L., Hu J., Tan R. B. H., Physical state and dissolution of ibuprofen formulated by cospray drying with mesoporous silica: Effect of pore and particle size, Int. J. Pharm. **2011**, 410, 188-195.

[14] Narayan R., Nayak U. Y., Raichur A. M., Garg S., Mesoporous Silica Nanoparticles: A Comprehensive Review on Synthesis and Recent Advances, *Pharmaceutics*, 10, 118 (1–49),**2018**

[15] Chircov C., Spoiala A., Ficai D., Mesoporous silica platforms with potential application in release and adsorption of active agents, *Molecules*, 25(17), 3814, **2020**

[16] Mei X., Chen D., Li N., Xu Q., Ge J., Li H., Lu J., Hollow mesoporous silica nanoparticles conjugated with pH-sensitive amphiphilic diblock polymer for controlled drug release, *Microporous and Mesoporous Materials*, 152, 16–24.,**2012**

[17] Pal N., Lee J-H., Cho E-B., Recent trends in morphology-controlled synthesis and application of mesoporous silica nanoparticles, *Nanomaterials*,*10(11),2122*, **2020**

[18] Ribeiro T., Rodrigues A. S., Calderon S., Fidalgo A., Gonçalves J. L. M., André V., Duarte M. T., Ferreira P. J., S. Farinha J. P., Baleizão C., Silica nanocarriers with user-defined precise diameters by controlled template self-assembly, *Journal of Colloid and Interface Science*, 561, 609–619,**2020**

[19] Stober W., Fink A., Bohn E., Controlled growth of Monodisperse Silica spheres in the micron size range ,*Journal of Colloid and Interface 26,62-69*, **1968**

[20] Raman I., Padavettan V., Synthesis of silica nanoparticles by sol-gel: size dependent properties, surface modification, and applications in silica polymer nanocomposites, *A review. Journal of nanomaterials* ,**2012**

[21] Narayan R., Usha Y. Nayak K., Ashok M. Raichur and Sanjay G., Mesoporous Silica Nanoparticles: A Comprehensive Review on Synthesis and Recent Advances, *Pharmaceutics,* 10(3),118,**2018**

[22] Chiang Y., Hong-yuan L., Sin-yen L., Controlling Particle Size and Structural Properties of Mesoporous Silica Nanoparticles Using the Taguchi Method, *The Journal of Physical Chemistry C*,115(27),13158-13165, **2011**

[23] Kwon S., Singh R.K., Perez R.A., Abou Neel E.A., Kim H.W., Chrzanowski W., Silica-based mesoporous nanoparticles for controlled drug delivery., *J Tissue Eng. 4: 2041731413503357,***2013**

[24] Popat A., Sandy Budi H., Frances S., Liu J., Mesoporous Silica Nanoparticles for Bioadsorption, Enzyme Immobilization, and Delivery Carriers, Nanoscale, 3(7):2801-18, **2011**

[25] Trewyn B. G., Slowing I. I., Giri S., Chen H., Lin V. S.-Y., Synthesis and Functionalization of a Mesoporous Silica Nanoparticle Based on the Sol – Gel Process and Applications in Controlled Release, *Acc. Chem. Res.* , 40 (9), 846–853,**2007**

[26] Dominik B., Post synthetic functionalization of mesoporous silica, *Nanoscle*,2(6),887-892, **2010**

[27] Hoffmann F., Fröba M., Vitalizing Porous Inorganic Silica Networks with Organic Functions—PMOs and Related Hybrid Materials, *Chem. Soc. Rev*,40(2),608-620, **2011**

[28] Lopes A.B.C., S. Farinha J.P., Baleizao C., Smart nanoparticles for controlled release applications, *Master thesis*, **2018**

[29] Slowing I., Trewyn B. G., and Lin V. S. Y., Effect of surface functionalization of MCM-41-type mesoporous silica nanoparticles on the endocytosis by human cancer cells, *J. Am. Chem. Soc*.,128(46),14792-14793, **2006**

[30] Grohganz H., Lobmann K., A Priemel P., Refining stability and dissolution rate of amorphous drug, *Pub Med expert opinion on drug delivery* 11(6), **2014**

[31] Beiner M., Pankaj S., Enke D., Steinhart M., Manipulating the crystalline state of pharmaceuticals by nanoconfinment, *Nano Lett*, 7, 5, 1381–1385,**2007**

[32] Graubner G., Anders N., Sonnenberger N., Steinhart M., Morphology of porous host directs preferred polymorh formation and influences kinetics of solid/solid transition of confined pharmaceuticals, *Cryst. Growth Des.,* 14, 1, 78–86,**2014**

[33] Khanfar M., Fares M. M., Qandil A. M., Mesoporous silica based macromolecules for dissolution enhancement of irbesartan drug using pre-adjusted pH method, *Microporous Mesoporous Mater***.** 173, 22-28,**2013**

[34] Tipduangta P., Takieddin K., Fabian L., Belton P., Qi S., Towards controlling the crystallisation behaviour of fenofibrate melt: triggers of crystallisation and polymorphic transformation*, RSC Advances***,** 8, 13153–13525,**2018**

[35] Di Martino P., Palmieri G.F., Martelli S., Evidence of a metastable form of fenofibrate, *Pharmazie* 55(8):625-6, **2000**

[36] Zhou D., Zhang G. G. Z., Law D., Grant D. J. W., Schmitt E. A., Physical stability of amorphous pharmaceuticals: Importance of configurational thermodynamic quantities and molecular mobility, *J. Pharm. Sci.*, 91(8), 1863–1872, **2002**

[37] Sailaja U., Thayyil M. S., Kumar N. S. K., Govindaraj G., Molecular dynamics of amorphous pharmaceutical fenofibrate studied by broadband dielectric spectroscopy, *Journal of Pharmaceutical Analysis*, 6(3), 165-170,**2016**

[38] Diogo H. P., Viciosa M.T., Moura Ramos J. J., Differential scanning calorimetry and thermally stimulated depolarization currents study on the molecular dynamics in amorphous fenofibrate, *Thermochimica Acta***,** 623, 29–35,**2016**

[39] Ling H., Luoma J.T., Hilleman D., A review of currently available fenofibrate and fenofibric acid formulations, *Cardiol. Res.*, 4 (2), 47–55,**2013**

[40] Ganesh P. Sanganwar, Ram B. Gupta, Dissolution-rate enhancement of fenofibrate by adsorption onto silica using supercritical carbon dioxide*, International Journal of Pharmaceutics*, 360, 213–218**,2008**

[41] Jia Z., Lin P., Xiang Y., Wang X and J, Zhang X and Q., A novel nanomatrix system consisted of colloidal silica and pH-sensitive polymethylacrylate improves the oral bioavailability of fenofibrate, *European Journal of Pharmaceutics and Biopharmaceutics*, 79, 126–134,**2011**

[42] Quan G., Wua Q, Zhanga Z., Zhana Z., Zhoua C., Chen B., Zhang Z., Li G., Pan X., Wu C., Enhancing in vitro dissolution and in vivo bioavailability of fenofibrate by solid self-emulsifying matrix combined with SBA-15, *Colloids and Surfaces B: Biointerfaces*, 141, 476–482,**2017**

[43] Vallet-Regi M.,Tamanoi F., Mesoporous Silica-based Nanomaterials and Biomedical Applications, Part A, *The Enzymes**, volume 43,1-10,* **2018**

[44] Lavilla Gomez M.D.C., synthesis and characterization of pH stimuli-responsive mesoporous silica nanoparticles, *PhD Thesis*, **2016**

[45] Taenho K., Jang I., surface modification of silica nanoparticles using phenyl trimethoxy silane and their dispersion stability in N-methyl-2-pyrrolidone, colloids and surfaces, *A: Physiochem. Eng. Aspects* 501,24-31**, 2016**

[46] Rosenholm M., Sahlgren J., Linden M., Multifunctional Mesoporous Silica Nanoparticles for Combined Therapeutic*, Diagnostic and Targeted Action in Cancer Treatment. Curr. Drug Targets*, 12 (8), 1166–1186.,**2011**

[47] Limnell T., Riikonen J., Salonen J.,Kaukonen A.M.,Laitinen L., Hirvonen J., Lehto V.P., Surface chemistry andpore size affect carrier properties of mesoporous silicon microparticles, *International Journal of Pharmaceutics*, 343:141–7**,2007**

[48] Hong S., Shen S.,Tan D.C.T., Ng W.K., Liu X., Chia L.S.O., Irwan A.W., Tan R., Nowak S.A., Marsh K., Gokhale R., High drug load, stable, manufacturable and bioavailable fenofibrate formulations in mesoporous silica: a comparison of spray drying versus solvent impregnation methods, *Drug Delivery*, 23(1), 316–327,**2016**

[49] Khodaverdi E., Ahmadi M., Kamali, H., Hadizadeh F., Aminopropyl groups of the functionalized Mobil Crystalline Material 41 as a carrier for controlled diclofenac sodium and piroxicam delivery,*J Pharm Investig*. Oct-Dec; 7(4): 174–181,**2017**

[50] Blin J.L, Gérardin C., Rodehüser L., Selve C., Stébé M. J, Influence of alkyl peptidoamines on the structure of functionalized mesoporous silica, *Chemistry of Materials*, 16(24), 5071–5080,**2004**

[51] She X., Chen L, Li C., He C, He L., Kong L., Functionalization of hollow mesoporous silica nanoparticles for improved 5-FU loading, research article*. journal of nanomaterial,* volume, ID 872035,**2015**

[52] Coates J., interpretation of infrared spectra, a practical approach*, Encyclopedia of Analytical Chemistry: applications, theory and instrumentation*, pp.10815-10837,**2000**

[53] Arkles B., Larson G., Book: silicon compounds silanes & silicones, 3rd chapter infrared analysis of organosilicon compounds, pp.175-178,**2013**

[54] Crucho I.C., Beleizao C., Farinha J.P.S., Functional group coverage and conversion quantification in nanostructured silica by 1H-NMR, *Anal. Chem., 89(1),681-687***,2016**

[55] Gunasekaran S., Devi T.S.R., Sakthivel P.S., Qualitative and Quantitative Analysis on Fibrates - A Spectroscopic Study, *Asian Journal of Chemistry*, 20(6), 4249-4268,**2008**

[56] Shi X.,Shao Y.,Sheng X., A New Polymorph of Fenofibrate Prepared by Polymer- mediated Crystallization, *Journal of Crystal Growth*,498, 93-102.**2018**

[57] Heinz, A., Gordon, K. C., McGoverin, C. M., Rades, T., Strachan, C. J., Understanding the solid-state forms of fenofibrate – A spectroscopic and computational study, European *Journal of Pharmaceutics and Biopharmaceutics* 71, 100–108, **2009**.

[58] Alhalaweha A., Alzghoulb A., Mahlina D., Bergströma C. A.S., Physical stability of drugs after storage above and below the glass transition temperature: Relationship to glass-forming ability, *Int journal of pharmaceutical*, volume 495, Pages 312-317, **2015**

[59]Fulcher G.S., Analysis of Recent Measurements of the Viscosity of Glasses, *J. Am. Ceram. Soc*., 8, 339–355,**1925**

[60] Avramov I., Viscosity in disordered media, *Journal of Non Crystalline Solids*, vol. 351, no. 40–42, pp. 3163–3173, **2005**.

[61] Brás A.R., Fonseca I.M., Dionísio M., Schönhals A., Affouard F., Correia N.T., Influence of Nanoscale Confinement on the Molecular Mobility of Ibuprofen, *Journal of Physical Chemistry*, 118(25), 13857–13868,**2014**

[62] Inocêncio S., Cordeiro T., Matos I., Danède F., Sotomayor J. C., Fonseca I. M., Correia N. T, Corvo, M. Dionísio M. C., Ibuprofen incorporated into unmodified and modified mesoporous silica: from matrix synthesis to drug release, *Microporous and Mesoporous Materials*,310, 110541, **2021**

[63] R. S.C.M.Q. Antonino, M. Ruggiero, Z. Song, T. L. Nascimento, E. M. Lima, A. Bohr, M. M. Knopp, K. Löbmann, *International Journal of Pharmaceutics*, 1, 100026, **2019**

[64] Watterson S., Hudson S., Svard M., Rasmuson A.C., Thermodynamics of Fenofibrate and Solubility in Pure Organic Solvents, *Fluid Phase Equilibria*,367,143-150, **2014**

[65] Gonçalves J. L., Crucho C.I., Alves S. P. C., Baleizão C., Farinha J.P.S., Hybrid Mesoporous Nanoparticles for pH-Actuated Controlled Release, *Nanomaterials*,9(3),483, **2019**